Received November 1, 2020, accepted November 12, 2020, date of publication November 17, 2020,
date of current version December 1, 2020.

*Digital Object Identifier 10.1109/ACCESS.2020.3038809*

# Analytical Formulation and Minimization of Voltage THD in Staircase Modulated Multilevel Inverters With Variable DC Ratios

**ELI BARBIE, (Student Member, IEEE), RAUL RABINOVICI, AND ALON KUPERMAN, (Senior Member, IEEE)**
School of Electrical and Computer Engineering, Ben-Gurion University of the Negev, Beer-Sheva 8410501, Israel
Corresponding author: Alon Kuperman (alonk@bgu.ac.il)

**ABSTRACT** Staircase Modulation (SCM) is a commonly employed switching strategy in Multilevel Inverters (MLI) with a high number of voltage levels ($N$). The main challenges in SCM are adjusting the Modulation Index (MI) to the desired value while minimizing the Total Harmonic Distortion (THD). This is achieved by solving an objective function for its optimum variables. These variables are the Switching Angles (SA) in the case of an MLI with Equal DC voltage Supply (EDCS), or both the SAs and the DC voltage supply Ratios (DCR), in the case of an MLI with Unequal DC voltage Supply (UDCS). Such an approach, which is referred to as Optimum Minimization of THD (OMTHD), relies on the accuracy of the THD expression used for the objective function. This paper reveals generic analytical closed-form formulations of both Phase-voltage THD (PTHD) for single-phase ($1\phi$) MLIs and Line-voltage THD (LTHD) for three-phase ($3\phi$) MLIs. The revealed THD expressions apply to SCM based MLIs of any topology, with either EDCS or UDCS voltage source configurations, which may be fixed or varying, and arbitrary value of $N$ (odd and even). Given an arbitrary $N$ value, the proposed unified formulations can be used to generate symbolic N-level PTHD or LTHD expressions, which are analytical functions of the SA and (optionally) DCR variables. The proposed THD expressions were used to form a generic OMTHD problem and solve for optimum SA and DCR variables, ensuring PTHD or LTHD minimization, subject to a set of optional constraints, such as the target MI, tolerable Modulation Error (ME), and the Maximum DCR (MDCR). Outcomes of the proposed OMTHD algorithm were successfully verified by Controller + Hardware-in-Loop (C-HIL) based experiments and compared against results of previous works, raveling significant improvement in THD accuracy and MLI's performance. A downloadable supplemental file containing Maple and MATLAB functions of the proposed THD expressions, as well as pre-calculated sets of optimum SAs and DCRs tables for 13 different values of $N$ ($4 \leq N \leq 16$), is provided for readers' convenience.

**INDEX TERMS** Multilevel inverters, staircase modulation, total harmonic distortion, optimization.

## I. INTRODUCTION

The important role of MLIs in power conversion applications is more than obvious [1]–[3]. One of the major challenges of MLI operation is output voltage THD minimization while maintaining desired MI [4]. This is achieved either by fundamental-frequency switching, such as SCM or by high-frequency control strategies, such as pulse width modulation (PWM) and space vector modulation (SVM) [4], [5]. While PWM and SVM may provide better overall performance, they may not be suitable for high power applications due to higher switching losses. SCM-based strategies such as square-wave modulation [4], selective harmonic elimination (SHE) [6], [7], or the more popular OMTHD [8]–[21] are often preferred due to their lower commutation burden (switching losses), especially for MLIs with a higher number of voltage levels ($N \geq 7$) [4], commonly employed in high power/voltage applications. The objective of OMTHD is obtaining target MI while minimizing PTHD or LTHD for $1\phi$-MLIs or $3\phi$-MLIs respectively. This is done by solving an objective function for optimum SAs in case of fixed EDCS or solving for both optimum SA and DCRs, in case of UDCS, with either fixed or varying voltages [4].

The use of UDCS may be intentional, e.g. used to increase the number of voltage levels ($N$) to switching devices ratio [15], consequently decreasing THD, or used to further

The associate editor coordinating the review of this manuscript and approving it for publication was Reinaldo Tonkoski.

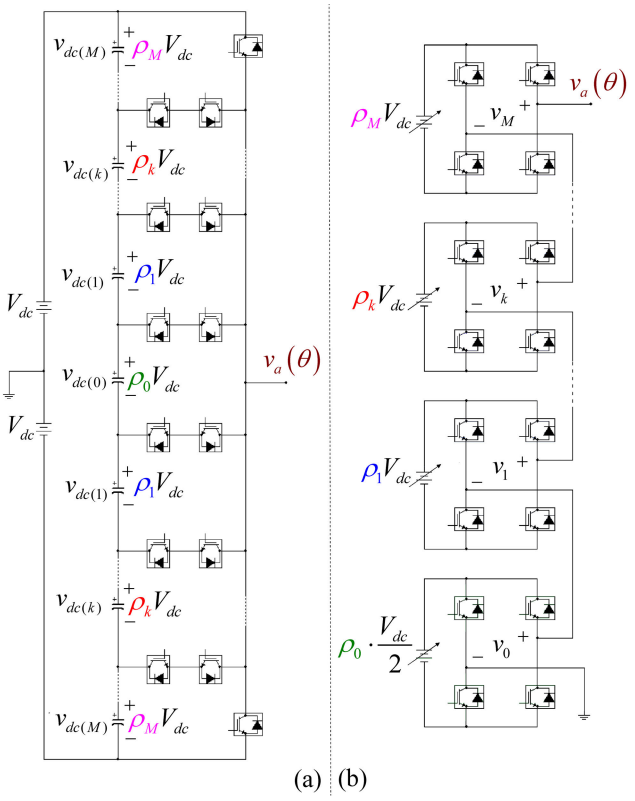


**FIGURE 1.** MLI Phase-Leg: (a) N-Level MPC, (b) N-Level CHB.

minimize the THD without increasing $N$ [16], [17]. UDCS may also be unintentional, caused by capacitor voltage variations, device voltage drops [18], or in renewable-energy-based DC supply, such as photovoltaic arrays, batteries, and fuel cells, in which rated voltage of each level may unintentionally vary [19].

MLIs generally fall into 3 main categories: **1)** Multipoint Clamped (MPC) with non-isolated dc sources, which include the diode-clamped MLIs [1]–[3] and the emerging T-type (''Nested'') MPCs [20]. These MLIs utilize a simple Single Pole Multiple Throw (SPMT) switch configuration (cf. Fig 1a) and are usually limited to EDCS only configurations, which may attain both odd and even values of $N$ [4]. MPC-based MLIs may also attain UDCS-based configurations, which may be unintentional due to voltage balancing variations and device voltage drops [18], [19], or intentional, in case the MLI is supplied by an active front-end, such as a multilevel rectifier (MLR) [22]. **2)** Cascaded H-bridge (CHB) with isolated dc sources (cf. Fig 1b) [4], [8]–[14]. These MLIs are often combined with SCM switching and may have balanced (EDCS) or unbalanced (UDCS) configurations. While CHB MLIs with even values of $N$ are uncommon, such configurations are theoretically feasible when UDCS is considered. This can be obtained by including one extra H-bridge cell with half the dc voltage, as depicted by the generic CHB phase-leg in Fig 1b (cf. Section 2.A). **3)** Other MLI topologies, such as Flying Capacitor Inverters (FCI) [21] and Modular Multilevel Converters (MMC) [7], [11] which may attain both EDCS and UDCS configurations, with either odd or even values of $N$.

Successful OMTHD implementation relies on the accuracy of the THD expression and proper scalarization of the objective function [23]–[26]. While several PTHD and LTHD formulations and minimizations addressing UDCS can be found in the literature [16]–[19], none of them are valid for even values of $N$, making them only applicable to CHB topologies. None of the previously proposed THD formulations was truly generalized closed-from, applicable to any value of $N$ and full MI range. For example, the real-time algorithm for PTHD minimization proposed in [19] for a 7-level 1$\phi$-MLI, is only valid for MI values greater than 0.55. Other generic UDCS-compatible LTHD expressions, valid for odd values of $N$ only, were revealed in [25]. The formulations were either open-form (involve unevaluated definite integrals), or recursively defined by a complex piecewise representation. A generic closed-form analytic formulation of PTHD, valid for both odd and even values of $N$ was recently revealed in [26]. However, this formulation is only applicable to 1$\phi$-MLIs and does not account for the UDCS cases. While references to higher (odd-only) $N$ values may be found in previously proposed OMTHD strategies [9]–[19], no true generic OMTHD, valid for any arbitrary value and parity of $N$ was provided until now. In most cases, PTHD and LTHD are usually calculated numerically in the frequency domain, accounting for at least 50 component harmonics [27], as per IEEE-519 and the revised IEEE-2014 standard recommendations [28]. This approach is prone to underestimation and rounding errors, consequently yielding sub-optimal results [27].

In this paper, generic and unified $N$-level analytic (closed-form) PTHD and LTHD expressions are revealed and then utilized in a generic N-level OMTHD to obtain a set of optimum SAs and (optionally) DCRs for any given value of the target MI, while maintaining a pre-defined tolerable ME and (optionally) MDCR. The proposed generic OMTHD solution, which is valid for SCM-based MLI's of any topology, with either EDCS or UDSC configurations, and any arbitrary value (or parity) of $N$, is obtained by offline global optimization (direct-search) algorithm. The optimum set of SAs $\alpha_1, \alpha_2, \ldots, \alpha_M$ and the optimum set of DCRs $\rho_0, \rho_1, \ldots \rho_M$ are calculated for a wide range of target MIs and stored as $M$ different Lookup Tables (LT) for multiple $N$ values ($7 \leq N \leq 16$). These LTs can then be used in an LT-based SCM controller. The calculated PTHD/LTHD results are compared against previously proposed methods, while OMTHD validation is carried out by C-HIL-based experiments, using 8 and 7-level MLI cases. A downloadable supplemental file that contains pre-programmed Maple and MATLAB PTHD/LTHD functions, some worked-out examples, and the pre-generated OMTHD LTs is provided for readers' convenience. The main outcomes and novelties of this research are highlighted as follows:

1. Mathematically-exact close-form THD expressions for both single and three-phase MLIs, with any number of voltage levels (odd or even).

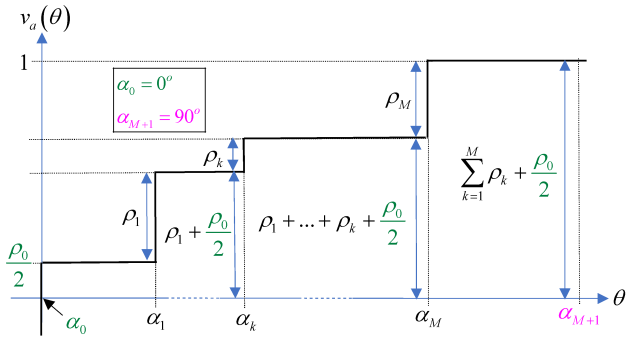


**FIGURE 2.** Generic normalized odd-quarter-wave symmetry SCM waveform (for odd and even *N* values).

2. A novel single-objective OMTHD algorithm with configurable modulation accuracy and maximum dc supply ratio.
3. Broad generic and unified THD and OMTHD formulations, applicable to MLIs of any topology with any dc voltage configurations (equal and unequal).

## II. GENERIC PHASE AND LINE VOLTAGE THD EXPRESSIONS

### A. BACKGROUND AND FORMULATIONS

A generalized N-level (odd or even) XDCS (namely, EDCS or UDCS, either fixed or varying) MLI's phase-leg of MPC, and equivalent CHB configuration, both having a total DC voltage of $2V_{dc}$, are presented in Fig 1a and 1b, respectively. The generic CHB phase-leg topology, depicted in Fig 1b, has one extra optional half-voltage $0^{\text{th}}$ cell corresponding to voltage step accruing at $\alpha_0 = 0^o$ (cf. Fig 2). This $0^{\text{th}}$ is only needed for even-$N$ values, resulting in a total of M+1 cells for an N-level MLI. While the proposed formulation is topology-independent (cf. Fig 1), the CHB structure is generally chosen due to its direct relation to SCM waveform generation. This is because the total number of voltage steps and consequently the number of SAs per quarter-wave, excluding the optional $\alpha_0$, is the same as the number of CHB cells ($M$). This quantity can be related to $N$, regardless of the parity of $N$, as [23], [24], [26]

$$M = \left\lfloor \frac{N-1}{2} \right\rfloor, \tag{1}$$

where $\lfloor\rfloor$ denotes the *floor* operator. Quarter-wave staircase waveform with odd-symmetry, corresponding to normalized (scaled by $V_{dc}^{-1}$) phase voltage output of the generic CHB leg (cf. Fig 1b), is presented in Fig 2. The generic SCM waveform consists of $M$ steps (1), each with a height of $\rho_k$ (normalized voltage step), occurring at a corresponding $k^{\text{th}}$ SA $\alpha_k$. In the case when $N$ is even, an extra step at the origin ($\alpha_0$) with a height of $\rho_0/2$ is also included.

Such generic SCM waveform can be represented by a unified expression, valid for both odd and even values of $N$ [24], [26]

$$v_a(\theta) = \sum_{k=1}^{M} \rho_k u(\theta - \alpha_k) + f_T \rho_0, \quad \begin{matrix} 0^o \le \theta \le 90^o \\ 0^o \le \alpha_k \le 90^o \end{matrix}, \tag{2}$$

where $\theta = \omega_1 t$ ($\omega_1$ signifying the base frequency), $\alpha_k$ with $k = 1 \ldots M$ is the $k^{\text{th}}$ SA in degrees, and

$$u(\theta - \alpha) = \begin{cases} 0, & \theta < \alpha \\ 1, & \theta \ge \alpha, \end{cases} \tag{3}$$

is the unit-step function, and $f_T$ is a parity toggle-function

$$f_T = \left\lfloor \frac{N}{2} \right\rfloor - \frac{N-1}{2} = \begin{cases} 0, & odd \\ 1/2, & even. \end{cases} \tag{4}$$

The voltage steps are normalized and weighed, vis

$$\sum_{k=1}^{M} \rho_k + f_T \rho_0 = 1, \quad 0 \le \rho \le 1. \tag{5}$$

For the symmetrical EDCS case, there is

$$\rho_0 = \rho_1 = \ldots = \rho_k = (M + f_T)^{-1} = 2/(N-1). \tag{6}$$

Using $f_T$ (4), the $\text{n}^{\text{th}}$ normalized harmonic component can also be unified for both odd and even values of $N$ [4], [24]

$$V_n = \frac{4}{\pi n} \cdot \left( \sum_{k=1}^{M} \left( \rho_k \cos\left( \frac{\pi n \alpha_k}{180} \right) \right) + f_T \rho_0 \right). \tag{7}$$

The normalized fundamental component, which serves as the modulation index (MI) is obtained by subsiding $n = 1$,

$$m_a = V_1 = \frac{4}{\pi} \cdot \left( \sum_{k=1}^{M} \left( \rho_k \cos\left( \frac{\pi \alpha_k}{180} \right) \right) + f_T \rho_0 \right). \tag{8}$$

Assuming balanced 3Φ load, line voltage MI is re-scaled as,

$$m_{ab} = \frac{\sqrt{3}}{2} \cdot m_a = \frac{2\sqrt{3}}{\pi} \cdot \left( \sum_{k=1}^{M} \left( \rho_k \cos\left( \frac{\pi \alpha_k}{180} \right) \right) + f_T \rho_0 \right) \tag{9}$$

resulting in a feasible MI ranges of

$$\begin{aligned} \frac{8}{\pi} \cdot \frac{f_T \rho_0}{N-1} \le m_a \le \frac{4}{\pi} = 1.27 \\ \frac{4\sqrt{3}}{\pi} \cdot \frac{f_T \rho_0}{N-1} \le m_{ab} \le \frac{2\sqrt{3}}{\pi} = 1.1. \end{aligned} \tag{10}$$

The root mean square (RMS) is generally defined as [4]

$$V_{rms} = \sqrt{\frac{1}{90} \int_0^{90} v_{scm}^2(\theta) d\theta}, \tag{11}$$

where $v_{scm}$ represents the staircase waveform. The percent THD expression (either phase or line) is defined as [4], [24]

$$THD = 100 \sqrt{\frac{2V_{rms}^2}{V_1^2} - 1}. \tag{12}$$

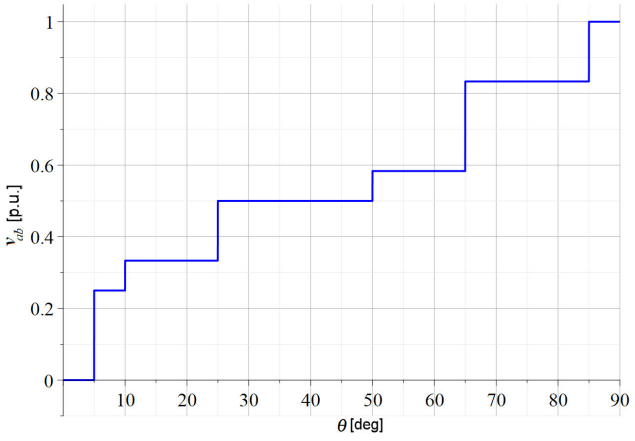


**FIGURE 3.** Example of a Normalized quarter-wave odd-symmetrical line-voltage SCM waveform ($M = 3$, $N = 7$, $\alpha_1 = 20^o$, $\alpha_2 = 35^o$, $\alpha_3 = 55^o$, $\rho_1 = 0.16, \rho_2 = 0.5, \rho_3 = 0.34$).

### B. CLOSED-FORM PTHD EXPRESSION

Squaring (11) and substituting $v_{scm}$ with $v_a(\theta)$ from (2),

$$V_{rms}^2 = \frac{1}{90}\int_0^{90} v_a^2 d\theta = \frac{1}{90}\int_0^{90}\left(\sum_{k=1}^{M}(\rho_k u(\theta-\alpha_k)) + f_T\rho_0\right)^2 d\theta,$$

expanding $v_a^2$ by applying the binomial theorem twice using double summation and simplifying as per the unit-step function properties, and rearranging, there is

$$v_a^2 = \sum_{k=1}^{M}\left(\left(2f_T\rho_0 + 2\sum_{i=1}^{k-1}\rho_i + \rho_k\right)\rho_k u(\theta-\alpha_k)\right) + (f_T\rho_0)^2.$$

Applying the internal integration of $V_{rms}^2$, there is

$$V_{rms}^2 = \frac{1}{90}\sum_{k=1}^{M}\left(\left(2f_T\rho_0 + 2\sum_{i=1}^{k-1}\rho_i + \rho_k\right)\rho_k(90-\alpha_k)\right) + (f_T\rho_0)^2.$$

The final PTHD expression is obtained by plugging (8) and the above $V_{rms}^2$ result in (12) and rearranging in (13), as shown at the bottom of the next page, where $M$ and $f_T$ are given by (1) and (4) respectively.

### C. CLOSED-FORM LTHD EXPRESSION

Recalling that the line voltage waveform leads the phase voltage waveform by a $30^o$ phase shift [4],

$$v_{ab}(\theta) = v_a(\theta) - \underbrace{v_a(\theta - 120^\circ)}_{v_b(\theta)},$$

where $v_a(\theta)$ is the quarter-wave odd symmetrical normalized phase voltage (2). Scaling $v_{ab}(\theta)$ by 1/2 to match the scale of the line voltage MI (9), then applying a $-30^o$ phase shift, using three $30^o$ segments in a piecemeal fashion, while acknowledging that $f(\theta) = -f(\theta \pm 180^o)$, the line voltage SCM waveform is re-centered as a normalized quarter-wave function with odd-symmetry (cf. Fig 3),

$$v_{ab}(\theta) = \frac{1}{2}\cdot\begin{cases} v_a(\theta+30^o) - v_a(30^o-\theta), & 0^o \le \theta < 30^o \\ v_a(\theta+30^o) + v_a(\theta-30^o), & 30^o \le \theta < 60^o \\ v_a(150^o-\theta) + v_a(\theta-30^o), & 60^o \le \theta \le 90^o. \end{cases} \quad (14)$$

Substituting $v_a(\theta)$ in (14) with its explicit form (2), there is

$$v_{ab}(\theta) = \begin{cases} f_1(\theta), & 0^o \le \theta < 30^o \\ f_2(\theta), & 30^o \le \theta < 60^o \\ f_3(\theta), & 60^o \le \theta \le 90^o, \end{cases} \quad (15)$$

with

$$\begin{aligned} f_1(\theta) &= \frac{1}{2}\sum_{k=1}^{M}(\rho_k\cdot(u(\theta-(30-\alpha_k)) \\ &\quad -u(-\theta+(\alpha_k-30)))) \\ f_2(\theta) &= \frac{1}{2}\sum_{k=1}^{M}(\rho_k\cdot(u(\theta-(\alpha_k-30)) \\ &\quad +u(\theta-(\alpha_k+30)))) + f_T\rho_0 \\ f_3(\theta) &= \frac{1}{2}\sum_{k=1}^{M}(\rho_k\cdot(u(\theta-(\alpha_k+30)) \\ &\quad +u(-\theta+(150-\alpha_k)))) + f_T\rho_0 \end{aligned} \quad (16)$$

The $V_{rms}^2$ term in (12), which is now assumed to be line-voltage, hence $v_{scm}(\theta) = v_{ab}(\theta)$, must be calculated in a piecemeal manner using (15) and (16).

$$V_{Lrms}^2 = \frac{1}{90}\left(\int_0^{30} f_1^2(\theta)d\theta + \int_{30}^{60} f_2^2(\theta)d\theta + \int_{60}^{90} f_3^2(\theta)d\theta\right). \quad (17)$$

To symbolically apply (17) with (16), the following two unit-step-function properties are considered

$$\begin{aligned} u(\theta-\alpha) &= \frac{d}{d\theta}\max(\theta-\alpha, 0) \\ u(\theta-\alpha) &= 1 - u(\alpha-\theta). \end{aligned} \quad (18)$$

Combining (18) with the following *min()* and *max()* function properties [30], where *mix()* denotes either *min()* or *max()*,

$$\begin{aligned} \min(x,y) &= -\max(-x,-y) \\ \mathrm{mix}(x,y) \pm z &= \mathrm{mix}(x\pm z, y\pm z), \end{aligned} \quad (19)$$

yields the following three unit-step function integration rules

$$\int_{\phi_1}^{\phi_2}(u(\theta-\lambda)\,u(\theta-\mu))d\theta = \phi_2 - \min(\max(\phi_1,\lambda,\mu),\phi_2)$$

$$\int_{\phi_1}^{\phi_2} (u(\theta-\lambda)\,u(-\theta+\mu))d\theta = \min(\phi_2,\mu) - \min(\max(\phi_1,\lambda),\phi_2,\mu).$$
$$\int_{\phi_1}^{\phi_2} (u(-\theta+\lambda)\,u(-\theta+\mu))d\theta = \max(\min(\phi_2,\lambda,\mu),\phi_1) - \phi_1 \quad (20)$$

Collecting (15) – (17), applying the binomial theorem and utilizing the commutativity and distributivity rules to each piece, eliminating sum products and sum squares, then simplifying using the properties from (18), followed by applying the integration rules of (20) and further simplifying using (19), the $2V_{Lrms}^2$ expression is finally obtained as

$$2V_{Lrms}^2 = N_1 + N_2 + N_3, \quad (21)$$

with

$$N_1 = \frac{1}{90}\cdot\sum_{i=1}^{M}\sum_{j=1}^{M} \times\left(\rho_i\rho_j\cdot\begin{pmatrix}\max(60-\alpha_j,0)+\min(0,60-\alpha_j)\\ -\max(\min(30,\alpha_i),60-\alpha_j,0)\\ +\max(0,\min(30,60-\alpha_i),\alpha_j-60)\\ +\max(\min(30,90-\alpha_i,30-\alpha_j),0)\end{pmatrix}\right). \quad (22)$$

$$N_2 = \frac{1}{180}\sum_{i=1}^{M}\sum_{j=1}^{M} \times\left(\rho_i\rho_j\cdot\begin{pmatrix}\max(\min(30,30-\alpha_i,30-\alpha_j),0)\\ +\max(\min(30,60-\alpha_i,60-\alpha_j),0)\\ +\max(\min(30,\alpha_i-30,\alpha_j-30),0)\\ +\min(30,90-\alpha_i,90-\alpha_j)\\ +\min(30,\alpha_i,\alpha_j)\end{pmatrix}\right). \quad (23)$$

$$N_3 = \frac{f_T\rho_0}{45}\sum_{k=1}^{M} \times\left(\rho_k\cdot\begin{pmatrix}\max(\min(30,30-\alpha_k),0)\\ +\min(30,90-\alpha_k)\\ +\min(60,90-\alpha_k)\end{pmatrix}\right)+\frac{4}{3}f_T^2\rho_0^2. \quad (24)$$

By collecting (21), (9), and (12), the final unified LTHD expression is obtained,

$$LTHD = 100\cdot\sqrt{\frac{2V_{Lrms}^2}{m_{ab}^2}-1} = 100\cdot\sqrt{\frac{N_1+N_2+N_3}{m_{ab}^2}-1}, \quad (25)$$

where $m_{ab}, N_1, N_2, N_3, M$ and $f_T$ are given by (9), (22), (23), (24), (1), and (4), respectively.

## III. MINIMIZATION OF PHASE AND LINE VOLTAGE THD

### A. BACKGROUND

The OMTHD objective is to adjust the MI while maintaining as low voltage THD as possible [14], [19], [23]. The minimized THD could be either phase-voltage THD (PTHD) [9] or Line-voltage THD (LTHD) [14]. Given a target MI, the optimum set of SAs is calculated for the EDCS case [14], while both sets of optimum SAs and optimum DCRs must be calculated for the UDCS case [17].

A distinction should be made between OMTHD, in which the MI ($m_a$ or $m_{ab}$), is regulated to achieve the desired target value ($m_T$), and Minimum THD, in which optimum SAs (and DCRs) are calculated to obtain absolute Minimum THD (MTHD) without any restriction on the MI [9], [17], [14]. MTHD based SCM is usually employed with adjustable DC supply applications, such as photovoltaic systems with DC-DC pre-regulator [19], or grid-fed systems with active MLRs [22]. When UDCS based MLIs are involved, OMTHD may describe 2 possible configurations, one for intentional and one for unintentional UDCS cases:

A. Intentional UDCS: Both the SAs $(\alpha_1, \alpha_2, \ldots, \alpha_M)$ and an optimum set of DCR $(\rho_0, \rho_1, \rho_2, \ldots, \rho_M)$ serve as design variables and must be calculated to obtain target MI with minimum THD [17].

B. Unintentional UDCS: Only optimum SAs are calculated (serve as design variables), while the DCRs are imposed as a set of restrictions (serve as parameters). Such configuration is used to mitigate DC variations due to device voltage drops [18], or when the DC supply vary naturally, such as when a renewable energy source is used for DC supply [19].

While "configuration A" is the main focus of this article, "configuration B" as well as the EDCS configuration are also addressed for sake of generality.

### B. OMTHD PROBLEM FORMULATION

OMTHD is essentially a bi-objective optimization problem [9], [14], [23], in which the THD expression and a MI

$$PTHD = 100\sqrt{\frac{\frac{1}{90}\sum_{k=1}^{M}\left(\left(2f_T\rho_0\rho_k+2\rho_k\sum_{i=1}^{k-1}\rho_i+\rho_k^2\right)(90-\alpha_k)\right)+f_T^2\rho_0^2}{\frac{8}{\pi^2}\left(\sum_{k=1}^{M}\rho_k\cos\left(\frac{\pi\alpha_k}{180}\right)+f_T\rho_0\right)^2}-1}, \quad (13)$$

tracking error function are scalarized and combined, forming a bi-objective fitness function

$$f_{obj} = w_1 \cdot f_{THD} + w_2 \cdot |m_{cal} - m_T|\,, \tag{26}$$

where $f_{THD}$ is the THD expression, $m_T$, is the target MI value, $m_{cal}$ is the calculated (actual) MI, which can be either $m_a$ or $m_{ab}$ for 1Φ or 3Φ, respectively, and $w_1, w_2$ are the two scalarization weights. The problem with such conventional formulation (26) is difficulty choosing the values of the two weights, so both the THD and MI tracking error get equal priorities, regardless of the target MI. Improper scalarization can result in either suboptimal THD or suboptimal MI tracking error [22].

$$\varepsilon_m = 100 \cdot \left| \frac{m_{cal} - m_T}{m_T} \right|. \tag{27}$$

To tackle this problem, an alternative approach to the OMTHD problem formulation is proposed. Instead of using the conventional formulation (26), the THD expression is used as a non-scalarized single-objective function, while a separate Modulation Error (ME) expression, accounting for the target MI, serves as an inequality constrain. The ME expression is generally defined in (27), where $m_T$ is the target ME, and $m_{cal}$ is the calculated MI, which can be either $m_a$(8) or $m_{ab}$ (9) for PTHD or LTHD based OMTHD, respectively.

Problem (Config A):

$$\begin{cases} \text{Minimize:} & THD\,(\alpha, \rho) \\ \text{Subject to:} & \\ \text{a)} & 0^o \le \alpha_k \le \alpha_{k+1} \le 90^o \\ \text{b)} & 0 \le \rho_k \le 1 \\ \text{c)} & \sum_{k=1}^{M} \rho_k + f_T \rho_0 = 1 \\ \text{d)} & \varepsilon_m \le \varepsilon_T \\ \text{e)} & \dfrac{\max(\rho)}{\min(\rho)} \le MDCR \\ \text{with:} & \begin{cases} \alpha = \{\alpha_1, \alpha_2, \ldots, \alpha_M\} \\ \rho = \{\rho_0, \rho_1, \ldots, \rho_M\} \end{cases} \end{cases}. \tag{28}$$

The proposed OMTHD problem (''configuration A'') is generally defined in (28) for both 1Φ or 3Φ MLIs, where $THD\,(\alpha, \rho)$ is the unified THD expression, which can be either PTHD (13) or LTHD (25), for 1Φ or 3Φ-MLI respectively. The other 5 expressions in (28) (28a to 28e), are the set of the problem's conditions (restrictions), which must be met, with $\alpha$ and $\rho$ serving as the SA and DCR design variables, respectively. For ''configuration A'' (cf. Section 3.A), conditions (28a) and (28b) set the range and constraints for the two design variables. Condition (28c) sets the normalization constraint for the DCR variable, which also reduces the effective degree of freedom for the DCR variable by 1, hence further simplifying the problem by limiting the global search domain. Condition (28d) sets the desired maximum tolerable ME value ($\varepsilon_T$) constraints, eliminating the need for scalarization, where $\varepsilon_m$ is the calculated ME (27). The value of $\varepsilon_T$ is usually set to 1% for most practical applications [14]. Condition (28e) sets an important constraint to limit the max possible per-level DC source variation (the cell voltages in case of CHB MLI). By setting a maximum limit to the DC source ratio (MDCR, p.u.), only practical DCR values are allowed, which helps balance the thermal power losses across the MLI's components. The MDCR value can be set to any values from 1 (= EDCS mode) to infinity (= no DCR restriction).

Problem (Config B):

$$\begin{cases} \text{Minimize:}, & THD\,(\alpha, v)|_{v=\rho} \\ \text{Subject to:} & \\ \text{a),} & 0^o \le \alpha_k \le \alpha_{k+1} \le 90^o \\ \text{b),} & \rho = \{\rho_0, \rho_1, \ldots, \rho_M\} \\ \text{c),} & \varepsilon_m \le \varepsilon_T \\ \text{with:}, & \alpha = \{\alpha_1, \alpha_2, \ldots, \alpha_M\}. \end{cases} \tag{29}$$

The second and simpler OMTHD ''configuration B'' (cf. Section 3.A), is defined in (29), where the set of DCRs are treated as constraints instead of design variables. This configuration can be used to obtain optimum SAs when the DC source voltage values are enforced, as well as for the EDCS case, using (6). The proposed OMTHD problem described by (28) or (29), can be solved using any Direct-search based global optimization algorithm, such as MATLAB's ''Global Pattern Search'' (GPS) [31], which was the algorithm of choice in this work, since the GPS algorithm is less sensitive than the highly stochastic Genetic Algorithm (GA), commonly employed for OMTHD [14], [17]. The novel OMTHD problem is intended for offline calculation of optimum SA and (optionally) optimum DCRs. It applies to any MLI topology with any value of $N$ (odd or even), either EDCS or UDCS-based, making it a truly generic and unified OMTHD approach.

## IV. RESULTS AND DISCUSSION

### A. VALIDATING THE PTHD EXPRESSION

For the EDCS case, the PTHD expression (13) was validated against reported results from [26, Table 1], which are obtained for the Nearest Level Control (NLC) switching strategy [32]. The set of SA was calculated using [26, (15)] for 4 and 7-level cases. Calculations were carried out symbolically and numerically using (13). For the 7-level case, the calculated SAs were

$$\begin{aligned} \alpha &= \left\{ \frac{180}{\pi} \cdot arcsin\left(\frac{1}{6}\right), 30, \frac{180}{\pi} \cdot arcsin\left(\frac{5}{6}\right) \right\} \\ &= \{9.49, 30, 56.44\}\,, \end{aligned}$$

and the corresponding % PTHD was

$$\begin{aligned} &PTHD_7 \\ &= 300 \sqrt{\frac{4\pi^2 - \pi\, arcsin\left(\frac{1}{6}\right) - 5\pi\, arcsin\left(\frac{5}{6}\right)}{\left(3\sqrt{3} + \sqrt{35} + \sqrt{11}\right)^2} - \frac{1}{9}} \\ &= 12.22728710. \end{aligned}$$

**TABLE 1.** Proposed vs [4] LTHD results comparison, (deg, %).

| $N$ | $\alpha_1$ | $\alpha_2$ | Actual (symbolic) | Actual (numeric) | Ref [4] |
|---|---|---|---|---|---|
| 3 | 15 | - | $\frac{5}{9}\sqrt{\frac{3150\pi^2}{cos\left(\frac{\pi}{12}\right)^2}-32400}$ | 16.863 | 16.86 |
| 4 | 20 | - | $\frac{50}{9}\sqrt{\frac{69\pi^2}{\left(cos\left(\frac{\pi}{9}\right)+\frac{1}{2}\right)^2}-324}$ | 11.858 | 11.86 |
| 5 | $\frac{15}{2}$ | $\frac{45}{2}$ | $25\sqrt{\frac{6\pi^2}{\left(cos\left(\frac{\pi}{24}\right)+cos\left(\frac{\pi}{8}\right)\right)^2}-16}$ | 9.432 | 9.43 |

For the 8-level case, the calculated SAs (deg) were

$$\alpha = \left\{\frac{180}{\pi}\cdot arcsin\left(\frac{2}{7}\right), \frac{180}{\pi}\cdot arcsin\left(\frac{4}{7}\right), \frac{180}{\pi}\cdot arcsin\left(\frac{6}{7}\right)\right\} = \{16.60, 34.85, 58.99\},$$

and the corresponding % PTHD as shown at the bottom of the next page, Both results match the ones reported in [26]. Results reported in [19, Fig 9] for the 7-level case were used to validate the UDCS case. The set of SAs and (normalized) DCRs reported in [19] were

$$\alpha = \{14.90, 43.54, 82.50\}, \quad \rho = \{0.45, 0.32, 0.23\},$$

corresponding to a PTHD value of 16.53%, vs 16.55%, obtained using (13). The lower result of [19] is indicative of an underestimation error, which is expected with numerical THD calculation [26].

### B. VALIDATING THE LTHD EXPRESSION

For the EDCS case, the LTHD expression was validated against results reported in [4, Table 2], obtained numerically for a "square-wave" modulated $3\phi$-MLIs (another SCM switching approach). Symbolic and subsequent exact numerical LTHD calculations were obtained using (25), which are summarized in Table 1, along with matching results from [4]. For the UDCS case, the reported results for an 11-level MLI from [25, Table 3] were used for comparison. The SA and normalized DCR sets were

$$\alpha = \{15, 25, 40, 55, 60\}, \quad \rho = \{0.3, 0.25, 0.2, 0.15, 0.1\}$$

The corresponding LTHD result reported in [25] was 7.9194%. Using the proposed analytical LTHD expression, a matching result was obtained in $LTHD_{11}$, as shown at the bottom of the next page. Additional validations have revealed that when using FFT-based calculations, the number of harmonics had to be greater than $10^5$, so any underestimation error is eliminated.

### C. ABSOLUTE MINIMUM THD (MTHD)

Recalling from Section 3.A that MTHD is simply OMTHD with the ME restrictions lifted, so the optimum SAs and (optionally) DCRs are calculated based solely on absolute minimum THD. Both problem configurations "A" (28) and "B" (29), can be used to obtain MTHD optimal variables by lifting the ME and MDCR conditions, setting $\varepsilon_T$ and MDCR to a very large value ($eps^{-1}$ in MATLAB).

Fig 4 presents MTHD-based THD results of both PTHD and LTHD with EDCS and UDCS MLI configurations, presented against $N$. The results were obtained by solving the proposed generic OMLTHD problems in (27) and (28), using MATLAB's GPS algorithm. The corresponding MTHD based optimum variables are listed in Tables 2 to 6.

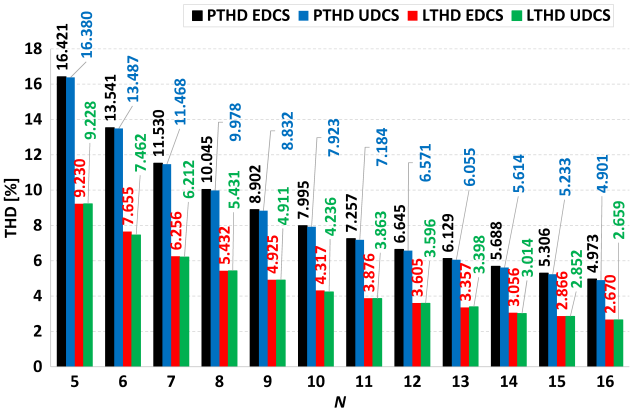


**FIGURE 4.** Phase and Line MTHD vs $N$.

**TABLE 2.** Optimum SAs for Line MTHD with EDCS (deg).

| $N$ | $\alpha 1$ | $\alpha 2$ | $\alpha 3$ | $\alpha 4$ | $\alpha 5$ | $\alpha 6$ | $\alpha 7$ |
|---|---|---|---|---|---|---|---|
| 4 | 21.13 | - | - | - | - | - | - |
| 5 | 7.84 | 24.16 | - | - | - | - | - |
| 6 | 13.09 | 34.49 | - | - | - | - | - |
| 7 | 5.38 | 16.33 | 34.22 | - | - | - | - |
| 8 | 9.20 | 18.66 | 34.05 | - | - | - | - |
| 9 | 4.00 | 12.08 | 20.42 | 33.94 | - | - | - |
| 10 | 7.27 | 14.66 | 26.29 | 39.25 | - | - | - |
| 11 | 3.24 | 9.78 | 16.44 | 26.93 | 38.52 | - | - |
| 12 | 5.88 | 11.83 | 17.91 | 27.47 | 37.97 | - | - |
| 13 | 2.73 | 8.23 | 13.81 | 22.45 | 31.67 | 41.93 | - |
| 14 | 5.03 | 10.09 | 15.24 | 23.23 | 31.72 | 41.09 | - |
| 15 | 2.32 | 6.98 | 11.69 | 16.47 | 23.90 | 31.79 | 40.42 |
| 16 | 4.36 | 8.75 | 13.18 | 20.01 | 24.71 | 32.14 | 43.17 |

**TABLE 3.** Optimum SAs for Phase MTHD with UDCS (deg).

| $N$ | $\alpha 1$ | $\alpha 2$ | $\alpha 3$ | $\alpha 4$ | $\alpha 5$ | $\alpha 6$ | $\alpha 7$ |
|---|---|---|---|---|---|---|---|
| 4 | 35.14 | - | - | - | - | - | - |
| 5 | 13.45 | 42.66 | - | - | - | - | - |
| 6 | 22.53 | 47.93 | - | - | - | - | - |
| 7 | 9.48 | 29.17 | 51.88 | - | - | - | - |
| 8 | 16.62 | 34.29 | 54.95 | - | - | - | - |
| 9 | 7.32 | 22.28 | 38.41 | 57.46 | - | - | - |
| 10 | 13.18 | 26.86 | 41.77 | 59.53 | - | - | - |
| 11 | 5.95 | 18.04 | 30.71 | 44.64 | 61.30 | - | - |
| 12 | 10.92 | 22.13 | 33.97 | 47.05 | 62.78 | - | - |
| 13 | 5.02 | 15.17 | 25.67 | 36.83 | 49.20 | 64.12 | - |
| 14 | 9.33 | 18.83 | 28.71 | 39.27 | 51.03 | 65.26 | - |
| 15 | 4.34 | 13.08 | 22.04 | 31.41 | 41.45 | 52.67 | 66.28 |
| 16 | 8.14 | 16.39 | 24.89 | 33.80 | 43.39 | 54.14 | 67.21 |

**TABLE 4.** Optimum DCRs for Phase MTHD with UDCS (p.u.).

| N | p0 | p1 | p2 | p3 | p4 | p5 | p6 |
|---|---|---|---|---|---|---|---|
| 4 | 0.7 | 0.65 | - | - | - | - | - |
| 5 | - | 0.52 | 0.48 | - | - | - | - |
| 6 | 0.43 | 0.41 | 0.37 | - | - | - | - |
| 7 | - | 0.35 | 0.34 | 0.30 | - | - | - |
| 8 | 0.31 | 0.30 | 0.29 | 0.26 | - | - | - |
| 9 | - | 0.27 | 0.26 | 0.25 | 0.22 | - | - |
| 10 | 0.24 | 0.24 | 0.23 | 0.22 | 0.19 | - | - |
| 11 | - | 0.22 | 0.21 | 0.21 | 0.19 | 0.17 | - |
| 12 | 0.20 | 0.20 | 0.19 | 0.19 | 0.17 | 0.15 | - |
| 13 | - | 0.18 | 0.18 | 0.18 | 0.17 | 0.16 | 0.14 |
| 14 | 0.17 | 0.17 | 0.16 | 0.16 | 0.15 | 0.14 | 0.13 |
| 15 | - | 0.16 | 0.15 | 0.15 | 0.15 | 0.14 | 0.13 |
| 16 | 0.15 | 0.15 | 0.14 | 0.14 | 0.14 | 0.13 | 0.12 |

**TABLE 5.** Optimum SAs for Line MTHD with UDCS (deg).

| N | α1 | α2 | α3 | α4 | α5 | α6 | α7 |
|---|---|---|---|---|---|---|---|
| 4 | 21.22 | | | | | | |
| 5 | 7.95 | 24.27 | - | - | - | - | - |
| 6 | 14.18 | 34.18 | - | - | - | - | - |
| 7 | 5.61 | 16.96 | 34.09 | - | - | - | - |
| 8 | 9.31 | 18.79 | 34.04 | - | - | - | - |
| 9 | 3.96 | 11.93 | 20.06 | 34.00 | - | - | - |
| 10 | 7.63 | 15.35 | 26.63 | 39.05 | - | - | - |
| 11 | 3.29 | 9.90 | 16.60 | 26.99 | 38.61 | - | - |
| 12 | 5.79 | 11.62 | 17.53 | 27.24 | 38.29 | - | - |
| 13 | 2.58 | 7.74 | 12.95 | 18.23 | 27.42 | 38.07 | - |
| 14 | 5.10 | 10.22 | 15.39 | 23.34 | 31.95 | 41.18 | - |
| 15 | 2.28 | 6.84 | 11.45 | 16.10 | 23.64 | 31.91 | 40.84 |
| 16 | 4.47 | 8.96 | 13.50 | 20.15 | 24.59 | 32.21 | 42.98 |

The EDCS-based optimum SA values for the PTHD and LTHD are listed in Tables 2 and 3, respectively. The UDCS-based optimum SAs and DCRs corresponding to the THD results of Fig 4 are listed in Tables 4 and 5 for the PTHD case and in Tables 6 and 7 for the LTHD case, respectively. The difference between EDCS and UDCS based MTHD, as shown in Fig 4, is not significant. Using UDCS instead of EDCS has decreased the PTHD and LTHD by up to 1.5% and 2.5% respectively. However, this is not the case for OMTHD, as it is shown in the upcoming subsections.

**TABLE 6.** Optimum DCRs for Line MTHD with UDCS (p.u.).

| N | p0 | p1 | p2 | p3 | p4 | p5 | p6 | p7 |
|---|---|---|---|---|---|---|---|---|
| 4 | 0.67 | 0.66 | - | - | - | - | - | - |
| 5 | - | 0.51 | 0.49 | - | - | - | - | - |
| 6 | 0.44 | 0.43 | 0.35 | - | - | - | - | - |
| 7 | - | 0.35 | 0.34 | 0.31 | - | - | - | - |
| 8 | 0.29 | 0.29 | 0.28 | 0.28 | - | - | - | - |
| 9 | - | 0.25 | 0.25 | 0.24 | 0.27 | - | - | - |
| 10 | 0.23 | 0.23 | 0.23 | 0.23 | 0.19 | - | - | - |
| 11 | - | 0.20 | 0.20 | 0.20 | 0.21 | 0.19 | - | - |
| 12 | 0.18 | 0.18 | 0.18 | 0.18 | 0.20 | 0.18 | - | - |
| 13 | - | 0.16 | 0.16 | 0.16 | 0.16 | 0.19 | 0.18 | - |
| 14 | 0.16 | 0.16 | 0.16 | 0.15 | 0.17 | 0.15 | 0.14 | - |
| 15 | - | 0.14 | 0.14 | 0.14 | 0.14 | 0.16 | 0.14 | 0.14 |
| 16 | 0.14 | 0.14 | 0.14 | 0.14 | 0.13 | 0.12 | 0.14 | 0.13 |

### D. OPTIMAL THD MINIMIZATION (OMTHD)

The proposed generic OMTHD configurations from (28) and (29) were programmed as MATLAB scripts, employing the GPS algorithm [31]. Optimum sets of SAs and optionally DCRs for 13 different values of $N$ were obtained for EDCS and UDCS (phase and line voltages), using 101 evaluated MI points per each $N$ value. The obtained OMTHD results are presented and discussed in this subsection. These results, as well as the pre-programmed Maple and MATLAB THD functions from (13) and (25), are all included in the supplemental file, available for download in [33].

#### 1) EQUAL DC SOURCES (EDCS)

Obtained minimum THD vs actual MI results are presented in Figures 5 and 6 for PTHD and LTHD respectively (odd-$N$ and even-$N$ cases were separated).

The target ME ($\varepsilon_T$) was set to 1%, and then verified using (27), confirming that the ME values ($\varepsilon_m$) remain within the specified limits. Fig 7 presents the actual ME results, corresponding to the odd-$N$ minimum LTHD results of Fig 6a, which shows that the actual ME approaches its maximum tolerable value from the left regardless of the target ME, namely $\varepsilon_m \rightarrow \varepsilon_T^-$. It should be noted that the feasible minimum THD results are highly sensitive to the actual ME, which is set by the restrictions in (28d) or (29c). The higher the ME,

$$PTHD_8 = 100\sqrt{\frac{\frac{49\pi^2}{32} - \frac{\pi}{2}arcsin\left(\frac{2}{7}\right) - \pi\, arcsin\left(\frac{4}{7}\right) - \frac{3\pi}{2}arcsin\left(\frac{6}{7}\right)}{\left(\frac{3\sqrt{5}+\sqrt{33}+\sqrt{13}}{7} + \frac{1}{2}\right)^2} - 1}$$
$$= 10.60564331.$$

$$LTHD_{11} = 100\sqrt{\frac{5717\pi^2}{5400\left(\frac{6}{5}cos\left(\frac{\pi}{12}\right) + cos\left(\frac{5\pi}{36}\right) + \frac{4}{5}cos\left(\frac{2\pi}{9}\right) + \frac{3}{5}cos\left(\frac{11\pi}{36}\right) + \frac{1}{5}\right)^2} - 1}$$
$$= 7.919360362.$$

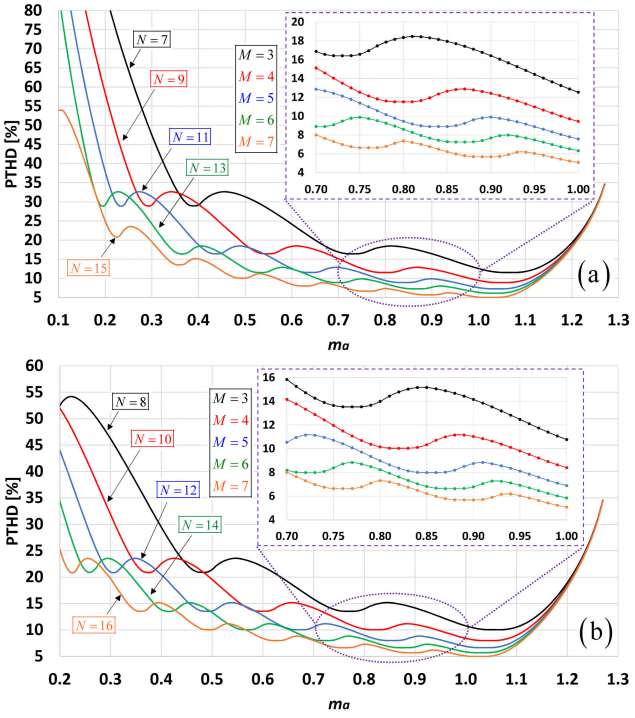


**FIGURE 5.** EDCS Minimum PTHD results vs MI: (a) Odd-*N*, (b) Even-*N*.

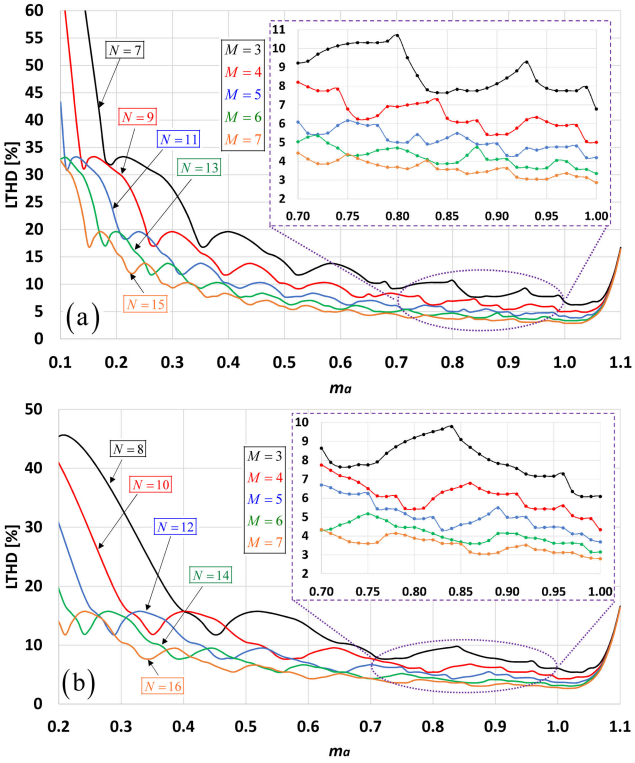


**FIGURE 6.** EDCS Minimum LTHD results vs MI: (a) Odd-*N*, (b) Even-*N*.

the lower the THD, and vice-versa, as it can be concluded from Fig 8, which highlights the impact of different target ME values on the PTHD results for $N = 7$. The obtained 7-level

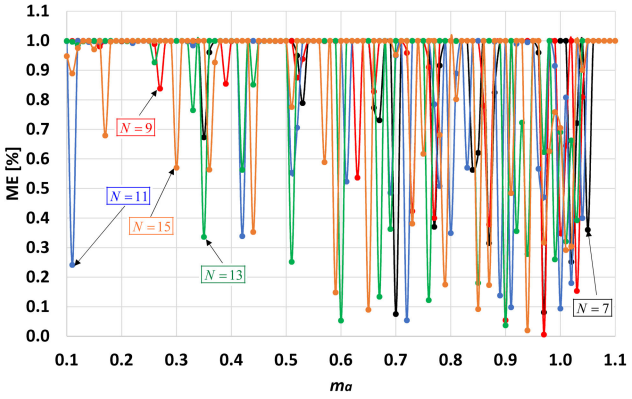


**FIGURE 7.** Calculated ME vs MI for Odd-*N* Minimum LTHD.

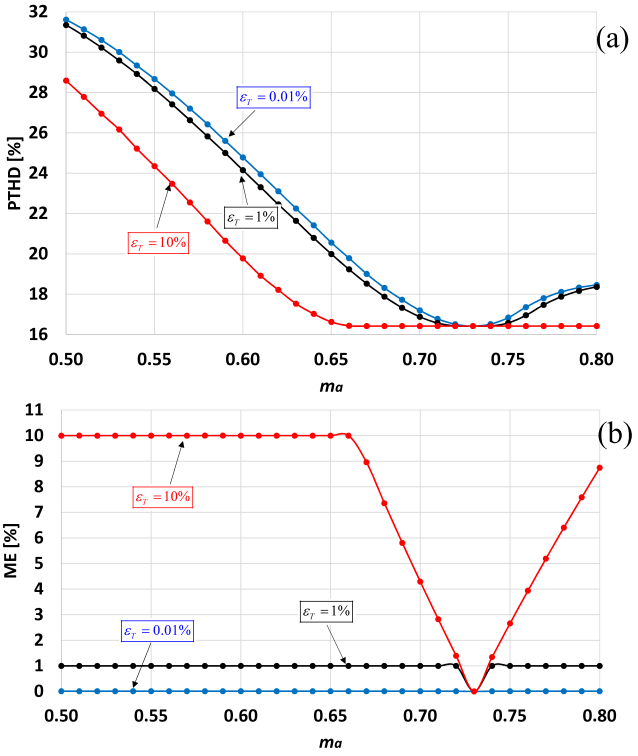


**FIGURE 8.** Impact of the target ME on Feasible Minimum THD values: (a) Minimum PTHD ($N = 7$) vs MI, (b) Calculated ME vs MI.

optimum SAs are shown in Fig 9a and Fig 9b for the minimum PTHD and LTHD respectively. Matching SA results from [14] are also included for reference. The corresponding PTHD and LTHD results are shown in Fig 10. As can be noted in Figures 9 and 10, the results of the proposed method are less sensitive and more "analytical" when compared to the results in [14]. These discrepancies are mainly attributed to the stochastic nature of the GA employed in [14], especially when the fitness function is not scalarized properly. The high computational burden imposed by the integral-dependent open-form THD expression used in [14], also plays a role in these sensitive results. The scalarization weights in [14] were

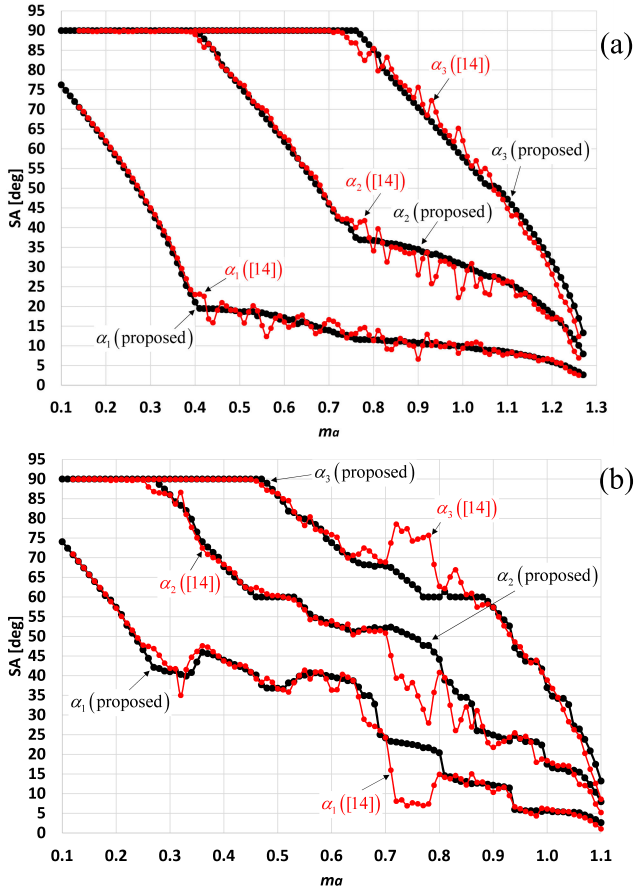


**FIGURE 9.** Comparison of 7-level optimum SAs: (a) Minimum PTHD, (b) Minimum LTHD.

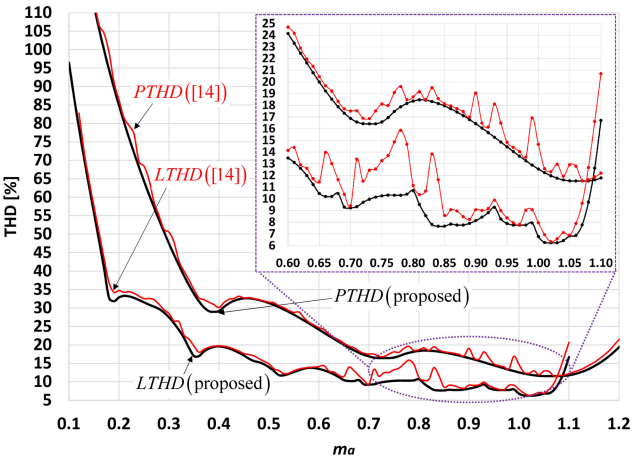


**FIGURE 10.** Comparison of 7-level THD results: proposed vs [14].

selected under the assertion that the LTHD value of the 7-level case is 10% while aiming for the desired ME of 1%. However, such an assertion is only valid for a specific value of MI and not the entire range. In the proposed OMTHD approach, the scalarization is eliminated, while the fitness function used is a true closed-form single-objective, which reduces the

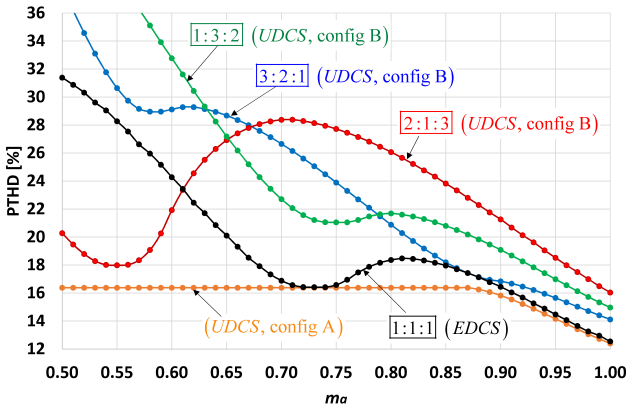


**FIGURE 11.** Comparison of 7-level Minimum PTHD results: EDCS vs UDCS ("configuration B") with different DCRs, vs optimal UDCS ("configuration A").

calculation burden, and consequently, the calculation errors. Another example of high sensitivity causing high fluctuations in the results can be observed in [10], where the GA was also employed for solving the OMTHD problem. The proposed PTHD results are lower than those obtained by [14] by up to 4%, while the proposed LTHD results are lower than the results of [14] by up to 6%, for the same ME results.

### 2) UNEQUAL DC SOURCES (UDCS)

UDCS generally refers to asymmetrical (unequal) MLI's DC sources, which may be either constant or varying. Two possible UDCS configurations were discussed in Section 3.B. The first, which was termed "configuration A", is defined by (28) and uses the full degree of freedom (both the SAs and the DCRs serve as the design variables). The second, which was termed "configuration B", is defined by (29) with only the SAs serving as the design variables, while the DC source ratios (DCR) serve as additional constraints.

Fig 11 presents a comparison of minimum PTHD results from different OMTHD configurations. It can be noted that different DCR setups (constraints) of the UDSC case with "configuration B" can have a significant impact on the feasible minimum THD value. For example, at $m_a = 0.5$, using a DCR of 2:1:3 (namely, $\rho_1 = 2/6$, $\rho_2 = 1/6$, and $\rho_3 = 3/6$) results in a lower THD value than DCRs of 1:3:2, 3:2:1, and 1:1:1 (the EDCS case), while at $m_a = 0.7$, a DCR of 1:3:2 yields better THD results than a DCR of 2:1:3. Clearly, for any given target MI value and DCR constraints, there exists a set of optimum SAs, which ensure minimum THD and a desired ME value. As expected, when both optimum SAs and DCRs are calculated ("configuration A" based UDCS setup), the lowest possible THD for any target MI value is obtained, which is apparent in Fig 11.

Real-time PTHD minimization for UDCS based MLIs was discussed in [19], which uses a single design variable to calculate the optimum set of SAs for odd-N only cases, given the desired DCRs ("configuration B" equivalent). The approach yields low, yet uncontrollable, ME (~0.001%). The problem

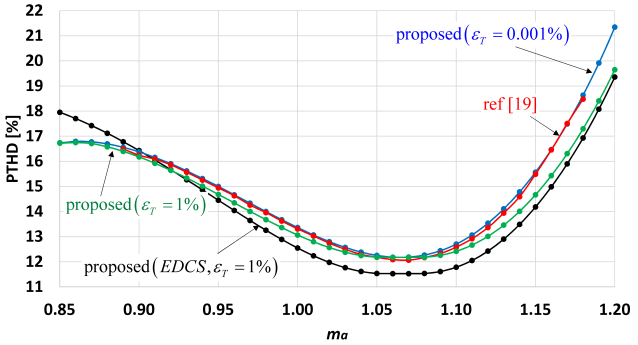


**FIGURE 12.** Comparison of 7-level Minimum PTHD results with UDCS ("configuration B", DCR = 1:0.7:0.5): Proposed vs [19].

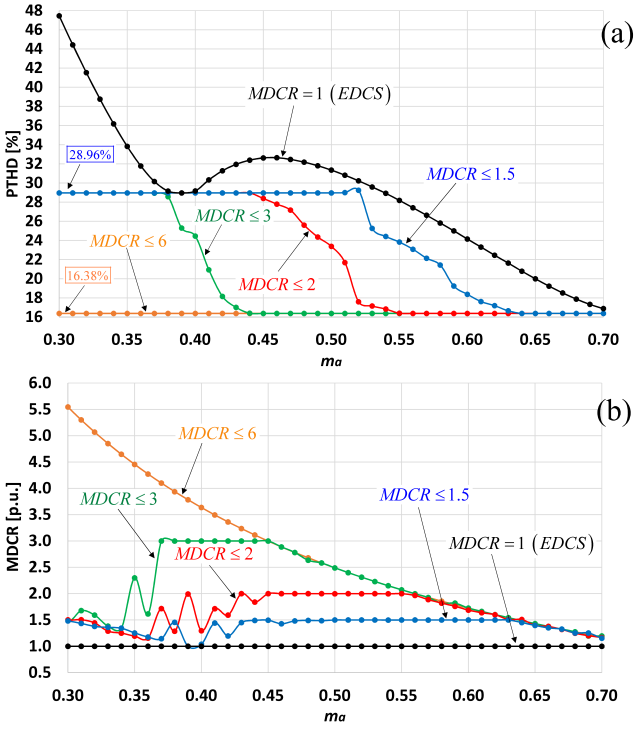


**FIGURE 13.** Proposed Phase voltage 7-level UDCS-based OMTHD results with different MDCR conditions: (a) PTHD, (b) MDCR.

with such an approach is with its MI range, which is limited to the upper range only ($m_a \geq 0.65$). Data for minimum PTHD of 7-level MLI with a DCR of 1:0.7:0.5 was extracted from [19] and then reproduced using the proposed OMTHD approach (configuration "B"), for different target ME values. The results, presented in Fig 12, highlight the advantage of the ability to control the amount of tolerated ME, consequently, achieving lower THD results.

Recalling from section 3.2, the MDCR restriction, defined by constraint (28e), limits the amount of allowed DC source variation (the maximum DC ratio). For the UDCS case, this parameter is inversely proportional to the feasible minimum THD, as it can be noted in the 7-level minimum PTHD results for different MDCR values in Fig 13a.

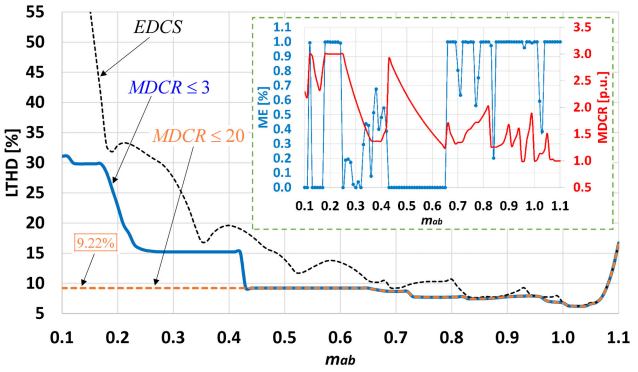


**FIGURE 14.** 7-level UDCS (configuration "A") results for MDCR ≤3: Minimum LTHD, ME, and actual MDCR values.

The corresponding actual MDCR values, calculated using the left-hand side of (28e), are presented in Fig 13b. As the target MDCR is increased (namely, DCR restrictions are loosened), the THD minimum can reach a lower value. For the 7-level case, an MDCR restriction of 6 yields a minimum PTHD of 16.38%, while an MDCR restriction of 3 results in a limited PTHD value of 28.96% (cf. Fig 13a). These values are not incidental, rather equivalent absolute minimum (MTHD) values of lower-order values of $M$. For the 7-level example in Fig 13, where $M = 3$, the PTHD result of 16.38% is equivalent to the obtained MTHD for the 5-level ($M = 2$) case (cf. Fig 4), while the 28.96% result is the 3-level ($M = 1$) MTHD result equivalent (cf. [26, Table 3 ]).

For sake of device stress equalization, it may be desirable to restrict the MDCR to a practical value of 3, especially for 7 and 8-level MLIs, where $M = 3$, resulting in a maximum scaled DCR of 1:2:3. Proposed OMTHD results (UDCS, configuration "A", $MDCR \leq 3$) for 3$\phi$-MLI are presented by Figures 14 - 15 and Figures 16 – 17 for 7-level and 8-level cases, respectively. EDCS based results are also included in Figures 13, 14, and 16 for reference.

Even with a conservative $MDCR \leq 3$ restriction, the reduction in LTHD is quite drastic, reaching 65% absolute difference for the 7-level case (cf. Fig 14) and an average reduction of 23.45% and 18.73%, across the entire MI range for the 7 and 8-level cases, respectively. Minimum LTHD results for a less restrictive $MDCR \leq 20$ case, are also included in Figures 14 and 16, which show even lower LTHD results especially at lower MI values (9.22% for 7-level and 7.46% for 8-level, as indicated in Figures 14 and 16, respectively). As previously discussed, these results which become stabilized for MI values roughly below 0.7, are the absolute minimum equivalent for $M = 2$ case, where the 9.22% minimum LTHD in Fig 14 is the same as the line voltage MTHD for the 5-level case, while the 7.46% minimum LTHD result in Fig 16 is the same as the line voltage MTHD for the 6-level case (cf. Fig 4).

The corresponding calculated (actual) ME and MDCR results for the $MDCR \leq 3$ case, are shown in the boxed areas of Figures 14 and 16 for the 7 and 8-level cases, respectively.

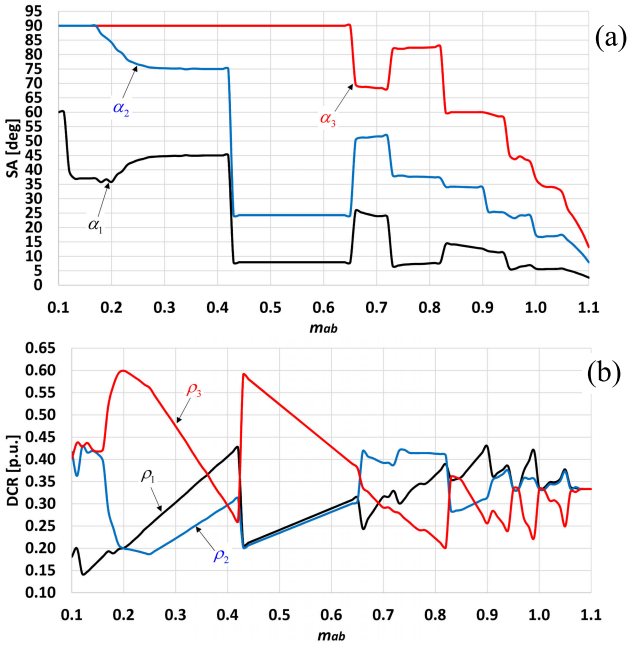


**FIGURE 15.** 7-level UDCS (configuration "A") results for MDCR ≤3: (a) SAs, (b) DCRs.

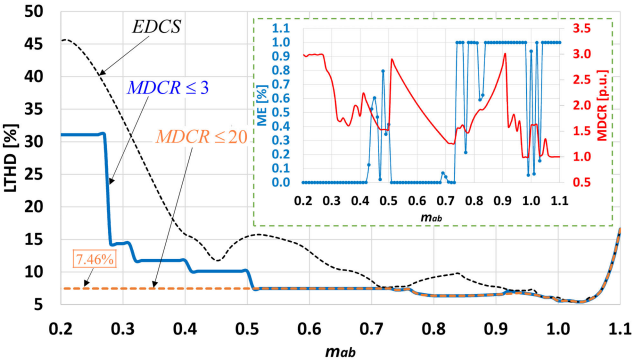


**FIGURE 16.** 8-level UDCS (configuration "A") results for MDCR ≤3: Minimum LTHD, ME, and actual MDCR values.

Both the ME and MDCR results remain within their specified restrictions of $\varepsilon_m \leq 1\%$ and $MDCR \leq 3$ for the full line voltage MI range ($0 \leq m_{ab} \leq 1.1$). Optimum sets of SA and DCR, corresponding for the $MDCR \leq 3$ minimum LTHD results are presented in Figures 15 and 17 for the 7 and 8-level cases respectively, which verify the remaining restrictions defined by (28a) to (28c).

The results, so far, show that when "configuration A" UDCS is permitted, nontrivial OMTHD solutions (for $N \geq 4$) can be obtained by adjusting the DCRs in addition to the SAs, to realize an optimal condition for a given target MI. However, once optimum DCRs are selected, practically speaking, their values should be held constant, since treating the DCRs as variables would imply expensive adjustable voltage DC supply for each voltage level. Namely, when $N$ is increased (especially above 7-levels), undesirable cost

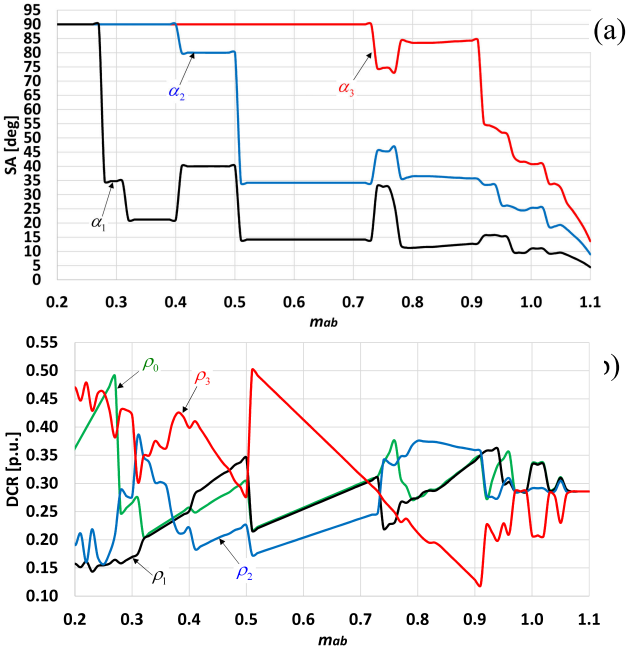


**FIGURE 17.** 8-level UDCS (configuration "A") results for MDCR ≤3: (a) SAs, (b) DCRs.

would be added to the system [4], [22]. Nevertheless, for MLIs with no more than 8-levels, in which the number of independently adjustable DC supplies is lower than 5, UDCS of "configuration A" may still be a practically feasible attractive solution [25]. An alternative solution would be to either use the "configuration B", in which the DCRs are set once, according to their MTHD-based optimum values (cf. Tables 2 to 6) or take advantage of the proposed MDCR restriction, by scarifying harmonic performance (THD) to reduce system's cost (or vice-versa). Similarly, the proposed ME restriction allows the sacrification of THD to increase modulation accuracy (or vice versa). These two intricate and unique features make the proposed OMTHD approach a true unified and generic OMTHD solution, applicable to any SCM based MLI.

### 3) UDCS WITH VARYING TOTAL DC VOLTAGE

A UDCS based OMTHD approach for a 7-level CHB MLI, in which the SAs DCRs, as well as the total DC voltage, were allowed to vary, was proposed in [17]. While this approach offered an additional degree of freedom, it suffered from high sensitivity, leading to erratic and sub-optimal results, which were due to 3 main problems related to the OMTHD formulation used in [17]: **1)** Lack of proper scalarization of the fitness function. The fitness function used in [17] is of the same conventional formulation defined in (26), with both scalarization weights set to unity: $w_1 = w_2 = 1$ (cf. [17, (8)]). **2)** The use of non-normalized DCR variables, namely: $\rho_1+\rho_2+\rho_3 \neq 1$. **3)** Improper setup of the GA parameters, yielding very sensitive and noisy results. By excluding the DCR normalization condition (28c) from the proposed

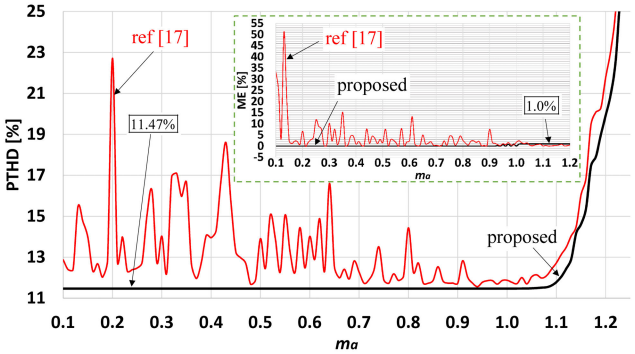


**FIGURE 18.** OMTHD results for 7-level UDCS with "Modified Configuration A": Minimum PTHD and calculated ME (boxed). Proposed approach vs [17].

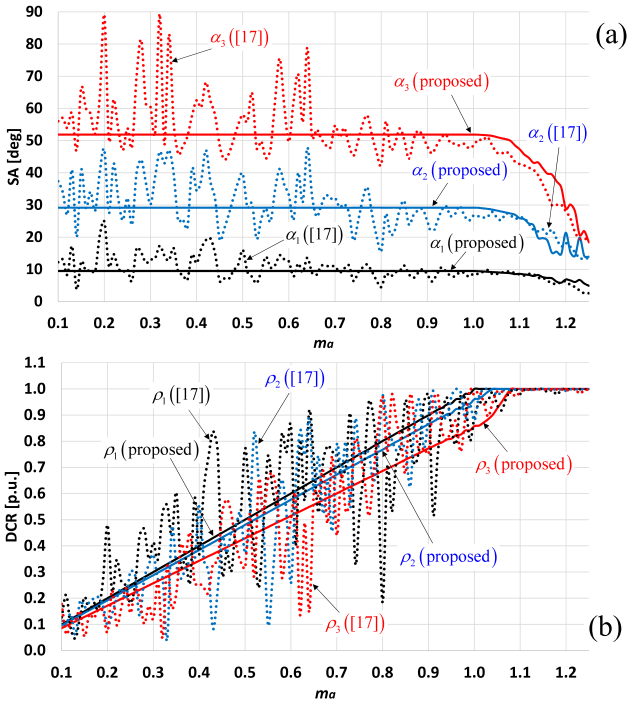


**FIGURE 19.** OMTHD results for 7-level UDCS with "Modified Configuration A". Proposed approach vs [17]: (a) SAs, (b) DCRs.

UDCS "configuration A" definition (28), the approach used in [17], which will be referred to as "modified configuration A", was successfully recreated with the adverse high sensitivity and high ME results of [17] eliminated. Data from [17, Fig 2] and [17, Fig 3] was extracted and used to recalculate both the PTHD and ME values. The results of [17] are presented in Figures 18 and 19, along with the proposed recreated results. As it can be noted in Fig 18, the recreated PTHD results are very consistent and stable at a fixed value of 11.47% (up to $m_a = 1.1$), which is the equivalent MTHD value for the 7-level case (cf. Fig 4), while the PTHD results from [17] are much higher and very erratic.

The corresponding comparison of the calculated ME, shown in the boxed area of Fig 18, reveals very high and

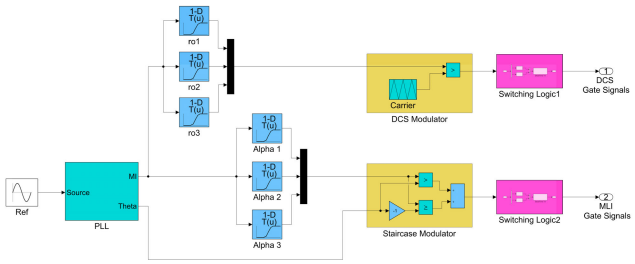


**FIGURE 20.** Conceptual per-phase functional diagram of the proposed SCM controller for a 7-level UDCS based MLI + DC Source Converter.

out of control ME results obtained by [17], reaching values of 50%, whereas the proposed recreation ME results remains within the specified 1% restriction. The optimum SAs and DCRs for both the original [17] and the recreated results are presented in Figures 18a and 18b respectively, revealing a strong correlation between the two approaches, despite the erratic behavior of the results obtained in [17]. The OMTHD approach employed in [17] is equivalent to setting both the SAs and DCRs at their absolute MTHD values, and then adjusting the MI by scaling all DC levels in a unison fashion, which explains why the recreated optimum SAs and DCRs in Fig 19 remains constant up to a certain MI point. The problem with such an approach is the unlimited DC source adjustment range, making it quite complex and expensive for most practical uses. An alternative approach would be to simply used the proposed OMTHD with the "configuration A" UDCS, then control the total DC voltage separately from the DC source's side. This way, both the MDCR and the DCR normalization restrictions can still be used to limit the DCR variations.

## V. VALIDATION

### A. SIMULATION BASED VALIDATION

By using the pre-generated optimum sets of SAs and DCRs, an LT-based SCM controller was modeled in Simulink. The per-phase functional diagram of the proposed 7-level UDCS based SCM controller is presented in Fig 20. The sinusoidal reference signal is used for the LT-based optimum SAs and DCRs generation, as well as for the DC source converter, which was based on a multi-output flyback converter [4].

In this simulation, CHB type 3Φ-MLI was modeled using the Simscape Power library. The MLI was loaded with a 120V (line) 60Hz 5kW induction motor load. The total DC voltage of the MLI was set to 120V ($3 \times 40V$ in case of EDCS operation). By emulating a Variable Frequency Drive (VFD) mode of operation (i.e. constant torque control), the sinusoidal reference signal was programmed so at $t = 0.4$ seconds into the simulation, the target MI ($m_T$) was decreased from 0.8 to 0.5, while the MLI's output frequency was increased by the reciprocal ratio, from *50Hz* to *80Hz*. To demonstrate the OMTHD's ability to ensure both accurate modulation and lowest LTHD possible, UDCS of "modified configuration A" was employed, in which the SAs, DCRs, as well as the total

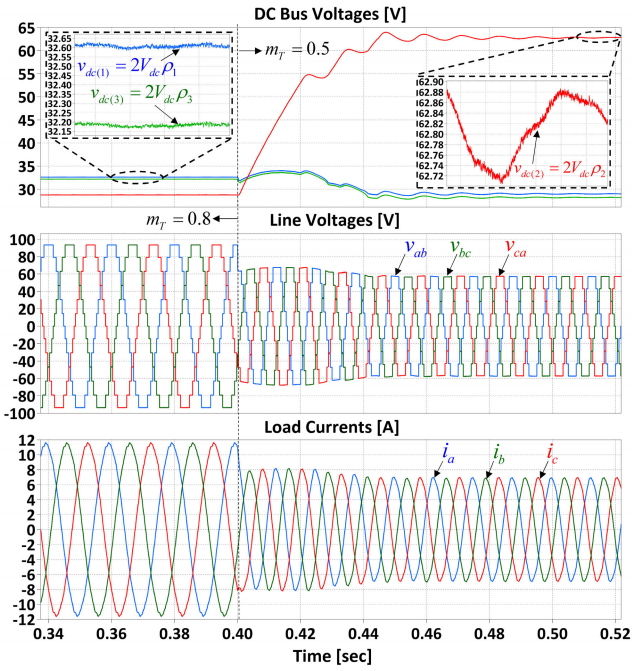


**FIGURE 21.** Simulation waveforms of 7-level UDCS based 3Φ-MLI with VFD emulation (Target MI change).

DC voltage, are allowed to vary. The 7-level VFD simulation results, which include 3 subplots (from top to bottom) **a)** the 3 DC bus voltages of the MLI (phase-leg A), **b)** the MLI's line voltages, and **c)** the motor's currents, are presented in Fig 21.

In this simulation, the MLI is switched from MTHD to OMTHD mode, by utilizing the full degree of freedom, namely, varying the total DC voltage ($2V_{dc}$), the SAs, and the DCRs. By varying the total DC voltage in addition to the SA and DCR variables, MTHD results can be obtained for virtually any desired MI, keeping the LTHD (or PTHD) at its absolute minimum value, which is 6.21% for the 7-level case (cf. Fig 4). Assuming that the highest MI value of $m_T = 1.1$ corresponds to a nominal total DC voltage of $V_{dc\_nom} = 120V$, and using the "modified configuration A" UDCS, for $t < 0.4$ sec, in which $m_T = 0.8$, then the MTHD-based optimum SA and DCR values, corresponding to $N = 7$, are simply obtained from Tables 5 and 6 as:

$$\alpha = \{\alpha_1, \alpha_2, \alpha_3\} = \{5.61^o, 16.96^o, 34.09^o\}$$
$$\rho = \{\rho_1, \rho_2, \rho_3\} = \{0.349, 0.344, 0.308\},$$

which according to (9), corresponds to an actual MI value of $m_{ab} = 1.026$. This value must then be adjusted (rescaled) according to the desired MI value of $m_T = 0.8$, by properly setting the target total DC voltage (cf. Fig 1), using the following calculation, which is automatically handled by the UDCS based SCM controller (cf. Fig 20):

$$2V_{dc} = V_{dc\_nom} \cdot \frac{m_T}{m_a} = 120 \cdot \frac{0.8}{1.026} = 93.57V.$$

For $t \geq 0.4$ sec, in which the target MI is reduced to $m_T = 0.5$, the optimum PS and DCR values are obtained by solving the "configuration A" OMTHD problem in (28) for both $\alpha$ and $\rho$, with $m_T = 0.5$, with $MDCR \leq 3.0$ and $\varepsilon_T \leq 1.0\%$ restrictions, which returns the following results:

$$\alpha = \{\alpha_1, \alpha_2, \alpha_3\} = \{7.95^o, 24.27^o, 90.00^o\}$$
$$\rho = \{\rho_1, \rho_2, \rho_3\} = \{0.242, 0.235, 0.523\}.$$

Recalling that the total DC voltage for $t < 0.4$ sec, in which MTHD-based SCM is employed, is 93.57V, therefore, the steady-stage average per cell DC values, in which $m_T = 0.8$, are as follows:

$$v_{dc(1)} = 2V_{dc} \cdot \rho_1 = 93.57 \cdot 0.349 = 32.65V$$
$$v_{dc(2)} = 2V_{dc} \cdot \rho_2 = 93.57 \cdot 0.344 = 32.18V$$
$$v_{dc(13)} = 2V_{dc} \cdot \rho_3 = 93.57 \cdot 0.308 = 28.82V.$$

For $t > 0.4$ sec, in which $m_T = 0.5$, the total DC voltage is changed back to its rated 120V value, and OMTHD-mode resumes, resulting in the following per-cell DC voltages:

$$v_{dc(1)} = 2V_{dc} \cdot \rho_1 = 120 \cdot 0.242 = 29.04V$$
$$v_{dc(2)} = 2V_{dc} \cdot \rho_2 = 120 \cdot 0.235 = 28.20V$$
$$v_{dc(13)} = 2V_{dc} \cdot \rho_3 = 120 \cdot 0.523 = 62.76V$$

All of the above results can be observed in Fig 21. A closer look at the phase-ab voltage output for the MTHD mode ($t < 0.4$ sec) is depicted in Fig 22. Another important takeaway from Figure 21, is the effective number of line voltage levels, which is at its maximum value of $2\times7-1 = 13$ for $t < 0.4$ sec (MTHD), while this value reduces to 10, for $t > 0.4$ sec. The obtained LTHD results for $m_T = 0.8$ and $m_T = 0.5$ are 6.21% and 9.23%, respectively, matching the expected results for the given SA and DCR values, as per the generic LTHD expression (25). These optimal LTHD values are significantly lower than the conventional EDCS or UDCS based OLTHD values for the given target MI values. For example, when $m_T = 0.8$, the OMTHD based LTHD values are 10.71% and 7.62% for the EDCS and UDCS cases, respectively. Similarly, when $m_T = 0.5$, the OMTHD based LTHD values are 13.96% and 9.23%, respectively. This means that utilizing the MTHD-based optimization by also adjusting the total DC voltage, improves the LTHD, compared to both EDCS and UDCS of "configuration A" based OMTHD approaches. Again, total DC voltage adjustment may add extra cost to the system, a factor that must be considered [4].

### B. EXPERIMENTAL (C-HIL) BASED VALIDATION

Real-world practical experiments involving multilevel converters with variable DC sources is quite challenging due to the required alterations in operating conditions, as well as safety when higher voltages are involved. This has led to other reliable validation solutions, such as the Hardware in Loop (HIL) and Controller + HIL (C-HIL), which has been gradually identified as an effective tool for power electronic converter development and digital control design, with

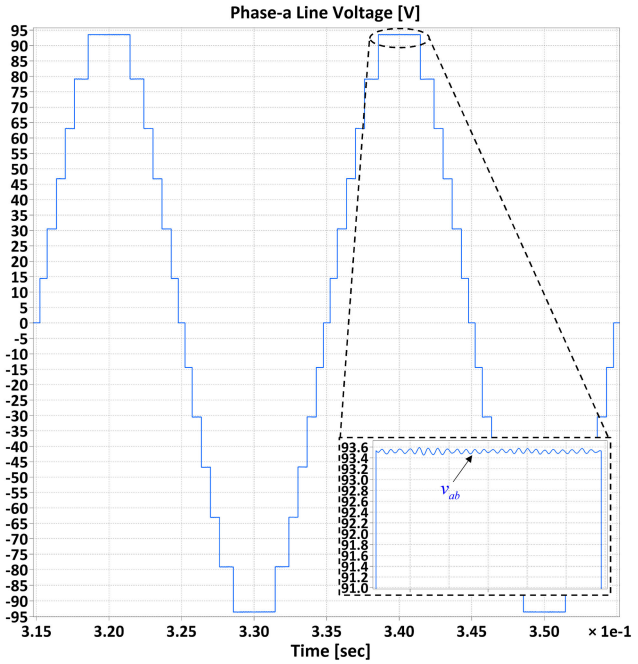


**FIGURE 22.** Line-voltage waveform of 7-level MTHD-optimized UDCS based 3Φ-MLI.

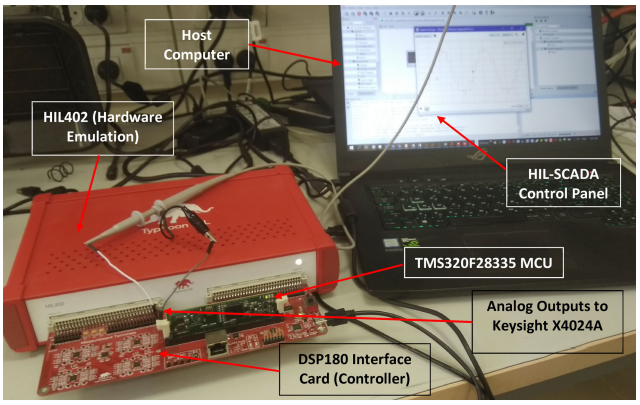


**FIGURE 23.** C-HIL Experimental setup.

near practical testing conditions [34], [35]. In this subsection, the proposed OMTHD is validated using the Typhoon HIL402 power-stage emulator [34], hosting the Typhoon DSP180 digital controller card (TMS32F28335 MCU based), namely, real-time emulations of both controller and MLI [35]. The experiments were based on both a simple 4-level and 7-level 3Φ-MLIs. A Keysight X4024A oscilloscope was used to capture, measure, and analyze the experimental voltage waveforms, generated by the HIL402.

The C-HIL setup which includes the HIL402, DSP interface card, and the host computer, running the HIL SCADA software, is depicted in Fig 23. Experiments for both phase and line voltage OMTHD were carried out using both 7 and 4-level MLIs, representing odd and even-N cases, respectively. 7-level (odd-N) results, obtained using the UDCS

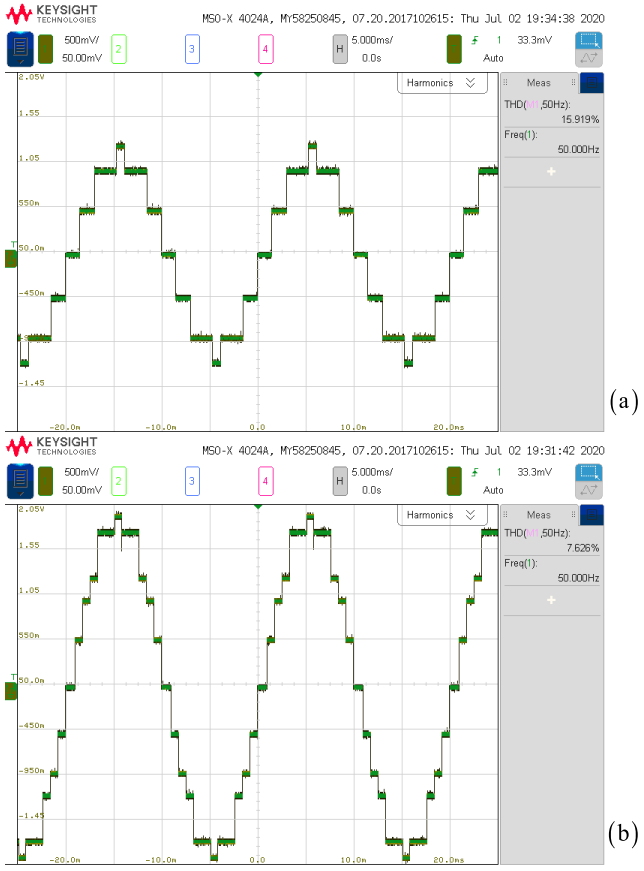


**FIGURE 24.** Experimental Voltage waveforms for 7-level 3$\phi$-MLI ($MDCR \leq 3$): (a) $v_a$ ($m_T = 0.891$), (b) $v_{ab}$ ($m_T = 0.772$).

of "configuration A", with $\varepsilon_T \leq 1\%$ and $MDCR \leq 3.0$ constraints, were compared against EDCS-based results, reported in [14], in which the values for the target MI were set to $m_T = 0.7 \cdot 4/\pi = 0.891$ for the phase-voltage OMTHD, and $m_T = 0.7 \cdot 2\sqrt{3}/\pi = 0.772$ for line-voltage OMTHD (the only experimental results specifically reported in [14]). The same MPC based 7-level 3$\phi$-MLI with a 50Hz reference signal and a 120V DC bus, supplying a 3kW balanced resistive load was used for phase and line-voltage optimizations.

The DSP code generation for the C-HIL was automatically generated using the Simulink SCM controller model (cf. Fig 20). The 7-level phase and line voltage waveform results are shown in Figures 24a and 24b, respectively.

Minimum THD, ME, and MDCR results, along with results from [14] for the 7-level experiments, are listed in Table 7, with the corresponding optimum SAs and DCRs (scaled by $1/\rho_{max}$) are listed in Table 8. Optimum variables with $MDCR \leq 3.0$ and two different ME restrictions for PTHD/ LTHD minimization, were calculated and compared against the EDCS-based results from [14]. The minimum PTHD for a target MI of 0.891 was 16.04% for $\varepsilon_T \leq 1\%$ and 16.22% for $\varepsilon_T \leq 10^{-4}\%$, a significantly lower than the 17.06% result obtained in [14]. Similarly, the minimum LTHD for a target MI of 0.772 was 7.70% for $\varepsilon_T \leq 1\%$ and

**TABLE 7. Results comparison of phase and line voltage minimum THD: Proposed (UDCS) vs [14] (EDCS).**

| Phase | PTHD [%] (Theoretical) | PTHD [%] (Experiment) | ME [%] | MDCR |
|---|---|---|---|---|
| **Ref [14]** | 17.06 | 17.07 | $1.59 \cdot 10^{-4}$ | 1.00 |
| **Proposed 1** | 16.04 | 15.92 | 1.0 | 1.64 |
| **Proposed 2** | 16.22 | 15.98 | $7.92 \cdot 10^{-5}$ | 1.74 |
| **Line** | **LTHD [%] (Theoretical)** | **LTHD [%] (Experiment)** | **ME [%]** | **MDCR** |
| **Ref [14]** | 10.31 | 10.23 | $5.68 \cdot 10^{-3}$ | 1.00 |
| **Proposed 1** | 7.70 | 7.64 | $2.01 \cdot 10^{-2}$ | 1.71 |
| **Proposed 2** | 9.41 | 9.12 | $5.59 \cdot 10^{-3}$ | 2.09 |

**TABLE 8. Results comparison of phase and line voltage THD-optimum SAs (deg) and DCRs (p.u.): Proposed (UDCS) vs [14] (EDCS).**

| Phase | $\alpha 1$ | $\alpha 2$ | $\alpha 3$ | $p1$ | $p2$ | $p3$ |
|---|---|---|---|---|---|---|
| **Ref [14]** | 10.34 | 34.61 | 72.95 | 1.00 | 1.00 | 1.00 |
| **Proposed 1** | 12.79 | 40.17 | 79.71 | 1.00 | 0.93 | 0.61 |
| **Proposed 2** | 12.99 | 40.95 | 82.24 | 1.00 | 0.92 | 0.58 |
| **Line** | $\alpha 1$ | $\alpha 2$ | $\alpha 3$ | $p1$ | $p2$ | $p3$ |
| **Ref [14]** | 21.81 | 47.75 | 60.06 | 1.00 | 1.00 | 1.00 |
| **Proposed 1** | 7.27 | 37.89 | 82.11 | 0.82 | 1.00 | 0.58 |
| **Proposed 2** | 21.49 | 53.19 | 66.81 | 1.00 | 0.84 | 0.48 |

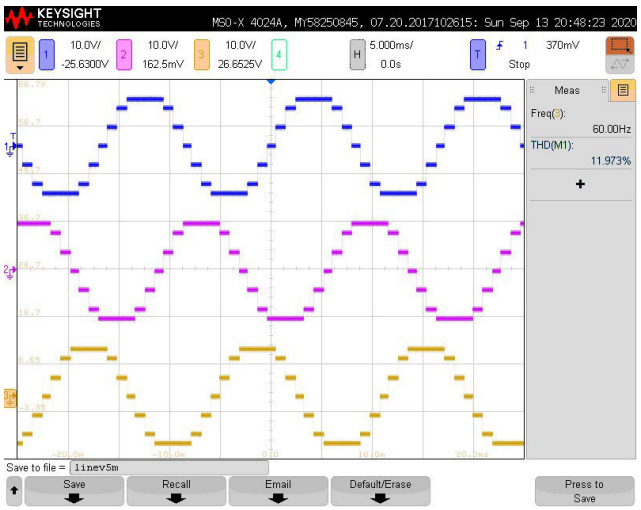


**FIGURE 25. Experimental Line Voltage waveforms for 4-level 3$\phi$-MLI (UDCS based MTHD).**

9.41% for $\varepsilon_T \leq 10^{-2}\%$, both of which are lower than the 10.31% results obtained in [14]. The calculated MDCR and ME values have remained within their specified limits. The FFT-based THD results, analyzed by the oscilloscope, were 15.92% (compared to 16.04% theoretical), and 7.63% (compared to 7.70% theoretical), for the PTHD and LTHD, respectively (cf. Fig 24). These minor differences are representative of the underestimation error, associated with numerical THD calculations [26].

Experimental results for a 4-level CHB MLI (even-N), obtained using the UDCS of "configuration B", with $\varepsilon_T \leq 1.0\%$ and MTHD-based optimum variables, extracted from Tables 5 and 6, respectively, are presented in Fig 25, which presents all 3 line-voltage waveforms of the 4-level MLI. The FFT-based LTHD calculation, in this case, was 11.97%, which is slightly higher than the expected theoretical result of 11.76% due to added PWM noise from the DC supply generation. For the 4-level case, only two cell DC voltages are needed. These voltages were generated using a dual output flyback converter. It should be noted that all experimental voltages are scaled down by a factor of 100:1 using the HIL SCADA Control panel.

## VI. CONCLUSION

The paper addressed the issue of analytic closed-form THD formulation and minimization in a broad generic approach, which is valid for all multilevel inverter (MLI) topologies, single-phase or three-phase, with equal/constant or unequal/varying DC sources and an arbitrary number of voltage levels ($N$), either odd or even. Novel analytical THD formulation and minimization approaches were derived for both phase (PTHD) and line (LTHD) voltage and then verified against numerically obtained results from previous works. The revealed unified THD expressions are capable of generating both symbolic results and mathematically-exact numerical results. The THD expressions, which are functions of the Switching Angles (SA) and the Ratio of the per-level DC sources (DCR), were implemented in a generic Optimal Minimization of THD (OMTHD), with an intricate and customizable set of conditions, such as the tolerable Modulation Error (ME) and the Maximum DCR (MDCR). OMTHD results for many different configurations were obtained for 13 different values of $N$. Variation of the total DC voltage, in addition to DCR variation, was also investigated, while the merits and demerits of each approach were discussed and evaluated. A downloadable supplemental file containing Maple and MATLAB source codes of the proposed THD expressions, as well as the pre-calculated sets of optimum SAs and DCRs, was provided. The OMTHD approaches for both PTHD and LTHD were verified by both simulations and Controller-Hardware-in-Loop (C-HIL) based experiments. Results were compared with previous works, verifying the proposed method's advantages in obtaining lower minimum THD without sacrificing the ME. The proposed generic and unified OMTHD methodology grants the freedom of prioritizing harmonic performance over modulation accuracy or system cost, and vice-versa.

## ABBREVIATIONS

| | |
|---|---|
| SCM | Staircase Modulation |
| MLI | Multilevel Inverter |
| MI | Modulation Index |
| THD | Total Harmonic Distortion |
| SA | Switching Angle |
| DCR | DC voltage Ratio |
| EDCS | Equal DC Sources |
| UDCS | Unequal DC Sources |

| | |
|---|---|
| OMTHD | Optimal Minimization of THD |
| PTHD | Phase voltage THD |
| LTHD | Line voltage THD |
| ME | Modulation Error |
| MDCR | Maximum DCR |
| HIL | Hardware in Loop |
| C-HIL | Controller + HIL |
| PWM | Pulse Width Modulation |
| SVM | Space Vector Modulation |
| MPC | Multipoint Clamped |
| CHB | Cascaded H-Bride |
| MMC | Modular Multilevel Converter |
| MLR | Multilevel Rectifier |
| LT | Lookup Table |
| MTHD | (Absolute) Minimum THD |
| GPS | Global Pattern Search |
| GA | Genetic Algorithm |
| VFD | Variable Frequency Drive |

## LIST OF SYMBOLS

| | |
|---|---|
| $N$ | Number of phase-voltage levels |
| $\phi$ | Phase |
| $M$ | Total number of SAs |
| $\alpha_k$ | $k^{th}$ SA value (in degrees) |
| $\rho_k$ | $k^{th}$ DCR value (in p.u.) |
| $f_T$ | Parity toggle function |
| $m_a$ | Phase voltage MI |
| $m_{ab}$ | Line voltage MI |
| $V_{rms}$ | Normalized RMS voltage |
| $v_a$ | Normalized phase voltage SCM signal |
| $v_{ab}$ | Normalized line voltage SCM signal |
| $\varepsilon_m$ | ME (in percent) |
| $2V_{dc}$ | Total DC voltage |

## ACKNOWLEDGMENT

The authors gratefully acknowledge the Typhoon HIL Inc. company for providing the C-HIL-based simulation platform.

## REFERENCES

[1] J. Rodriguez, L. G. Franquelo, S. Kouro, J. I. Leon, R. C. Portillo, M. Á. M. Prats, and M. A. Perez, "Multilevel converters: An enabling technology for high-power applications," *Proc. IEEE*, vol. 97, no. 11, pp. 1786–1817, Nov. 2009.

[2] J. Rodriguez, S. Bernet, B. Wu, J. O. Pontt, and S. Kouro, "Multilevel voltage-source-converter topologies for industrial medium-voltage drives," *IEEE Trans. Ind. Electron.*, vol. 54, no. 6, pp. 2930–2945, Dec. 2007.

[3] Y. He, Y. Liu, C. Lei, and J. Liu, "Equivalent space vector output of diode clamped multilevel inverters through modulation wave decomposition under carrier-based PWM strategy," *IEEE Access*, vol. 8, pp. 104918–104932, 2020.

[4] D. G. Holmes and T. A. Lipo, *Pulse Width Modulation for Power Converters: Principles and Practice*. Piscataway, NJ, USA: IEEE Press, 2003.

[5] P. Szczepankowski and J. Nieznanski, "Application of barycentric coordinates in space vector PWM computations," *IEEE Access*, vol. 7, pp. 91499–91508, 2019.

[6] M. Wu, H. Tian, Y. W. Li, G. Konstantinou, and K. Yang, "A composite selective harmonic elimination model predictive control for seven-level hybrid-clamped inverters with optimal switching patterns," *IEEE Trans. Power Electron.*, vol. 36, no. 1, pp. 274–284, Jan. 2021.

[7] Y. Xin, J. Yi, K. Zhang, C. Chen, and J. Xiong, "Offline selective harmonic elimination with (2N+1) output voltage levels in modular multilevel converter using a differential harmony search algorithm," *IEEE Access*, vol. 8, pp. 121596–121610, 2020.

[8] O. Lopez-Santos, C. A. Jacanamejoy-Jamioy, D. F. Salazar-D'Antonio, J. R. Corredor-Ramirez, G. Garcia, and L. Martinez-Salamero, "A single-phase transformer-based cascaded asymmetric multilevel inverter with balanced power distribution," *IEEE Access*, vol. 7, pp. 98182–98196, 2019.

[9] B. Diong, "THD-optimal staircase modulation of single-phase multilevel inverters," in *Proc. IEEE Region 5th Conf.*, San Antonio, CA, USA, Apr. 2006, pp. 275–279.

[10] V. Roberge, M. Tarbouchi, and F. Okou, "Strategies to accelerate harmonic minimization in multilevel inverters using a parallel genetic algorithm on graphical processing unit," *IEEE Trans. Power Electron.*, vol. 29, no. 10, pp. 5087–5090, Oct. 2014.

[11] A. R. Kumar, M. S. Bhaskar, U. Subramaniam, D. Almakhles, S. Padmanaban, and J. B.-H. Nielsen, "An improved harmonics mitigation scheme for a modular multilevel converter," *IEEE Access*, vol. 7, pp. 147244–147255, 2019.

[12] Y. Liu, H. Hong, and A. Q. Huang, "Real-time calculation of switching angles minimizing THD for multilevel inverters with step modulation," *IEEE Trans. Ind. Electron.*, vol. 56, no. 2, pp. 285–293, Feb. 2009.

[13] D. Hong, S. Bai, and S. M. Lukic, "Closed-form expressions for minimizing total harmonic distortion in three-phase multilevel converters," *IEEE Trans. Power Electron.*, vol. 29, no. 10, pp. 5229–5241, Oct. 2014.

[14] N. Yousefpoor, S. H. Fathi, N. Farokhnia, and H. A. Abyaneh, "THD minimization applied directly on the line-to-line voltage of multilevel inverters," *IEEE Trans. Ind. Electron.*, vol. 59, no. 1, pp. 373–380, Jan. 2012.

[15] A. A. K. Arani, H. R. Zaferani, M. J. Sanjari, and G. B. Gharehpetian, "Using genetic algorithm and simulated annealing for 27-level PV inverter THD minimization," in *Proc. Smart Grid Conf. (SGC)*, Tehran, Iran, Dec. 2014, pp. 1–6.

[16] H. Taghizadeh and M. Tarafdar Hagh, "Harmonic elimination of cascade multilevel inverters with nonequal DC sources using particle swarm optimization," *IEEE Trans. Ind. Electron.*, vol. 57, no. 11, pp. 3678–3684, Nov. 2010.

[17] N. Farokhnia, S. H. Fathi, N. Yousefpoor, and M. K. Bakhshizadeh, "Minimization of total harmonic distortion in a cascaded multilevel inverter by regulating voltages of DC sources," *IET Power Electron.*, vol. 5, no. 1, pp. 106–114, Jan. 2012.

[18] B. Diong, H. Sepahvand, and K. A. Corzine, "Harmonic distortion optimization of cascaded H-bridge inverters considering device voltage drops and noninteger DC voltage ratios," *IEEE Trans. Ind. Electron.*, vol. 60, no. 8, pp. 3106–3114, Aug. 2013.

[19] Y. Liu, H. Hong, and A. Q. Huang, "Real-time algorithm for minimizing THD in multilevel inverters with unequal or varying voltage steps under staircase modulation," *IEEE Trans. Ind. Electron.*, vol. 56, no. 6, pp. 2249–2258, Jun. 2009.

[20] E. C. D. Santos, J. H. G. Muniz, E. R. C. da Silva, and C. B. Jacobina, "Nested multilevel topologies," *IEEE Trans. Power Electron.*, vol. 30, no. 8, pp. 4058–4068, Aug. 2015.

[21] C. Sadanala, S. Pattnaik, and V. P. Singh, "A flying capacitor based multilevel inverter architecture with symmetrical and asymmetrical configurations," *IEEE J. Emerg. Sel. Topics Power Electron.*, early access, Oct. 8, 2020, doi: 10.1109/JESTPE.2020.3029681.

[22] E. Barbie, R. Rabinovici, and A. Kuperman, "Modeling and simulation of a novel active three-phase multilevel power factor correction front end—The 'Negev' rectifier," *IEEE Trans. Energy Convers.*, vol. 35, no. 1, pp. 462–473, Mar. 2020.

[23] E. Barbie, R. Rabinovici, and A. Kuperman, "Analytic formulation and optimization of weighted total harmonic distortion in single-phase staircase modulated multilevel inverters," *Energy*, vol. 199, May 2020, Art. no. 117470, doi: 10.1016/j.energy.2020.117470.

[24] E. Barbie, R. Rabinovici, and A. Kuperman, "Analytical formulation and optimization of weighted total harmonic distortion in three-phase staircase modulated multilevel inverters," *Energy*, vol. 215, Jan. 2021, Art. no. 119137.

[25] N. Farokhnia, H. Vadizadeh, S. H. Fathi, and F. Anvariasl, "Calculating the formula of line-voltage THD in multilevel inverter with unequal DC sources," *IEEE Trans. Ind. Electron.*, vol. 58, no. 8, pp. 3359–3372, Aug. 2011.

[26] E. Barbie, R. Rabinovici, and A. Kuperman, "Closed-form analytic expression of total harmonic distortion in single-phase multilevel inverters with staircase modulation," *IEEE Trans. Ind. Electron.*, vol. 67, no. 6, pp. 5213–5216, Jun. 2020.
[27] K. Omirzakhov and A. Ruderman, "Time domain optimization of voltage and current THD for a three-phase cascaded inverter with three H-bridges per phase," in *Proc. Int. Conf. Optim. Electr. Electron. Equip. (OPTIM) Intl Aegean Conf. Electr. Mach. Power Electron. (ACEMP)*, Brasov, Romania, May 2017, pp. 765–770.
[28] *IEEE Recommended Practice and Requirements for Harmonic Control in Electric Power Systems*, IEEE Standard 519-2014 (Revision of IEEE Std 519-1992), Jun. 2014, pp. 1–29.
[29] C. Dhanamjayulu, G. Arunkumar, B. J. Pandian, C. V. R. Kumar, M. P. Kumar, A. R. A. Jerin, and P. Venugopal, "Real-time implementation of a 31-level asymmetrical cascaded multilevel inverter for dynamic loads," *IEEE Access*, vol. 7, pp. 51254–51266, 2019.
[30] K. H. Rosen and J. G. Michaels, *Handbook of Discrete and Combinatorial Mathematics*. Boca Raton, FL, USA: CRC Press, 1999.
[31] N. Gunantara, "A review of multi-objective optimization: Methods and its applications," *Cogent Eng.*, vol. 5, no. 1, Jul. 2018, Art. no. 1502242.
[32] M. H. Nguyen and S. Kwak, "Nearest-level control method with improved output quality for modular multilevel converters," *IEEE Access*, vol. 8, pp. 110237–110250, 2020, doi: 10.1109/ACCESS.2020.3001587.
[33] *Suplemental File*. Accessed: Nov. 18, 2020. [Online]. Available: http://bit.ly/SUPF2
[34] *Typhoon HIL402 Bochure*. Accessed: Nov. 18, 2020. [Online]. Available: https://www.typhoon-hil.com/doc/products/Typhoon-HIL402-brochure.pdf
[35] *DSP180 Brochure*. Accessed: Nov. 18, 2020. [Online]. Available: https://www.typhoon-hil.com/doc/brochures/HIL-DSP-180-Interface.pdf

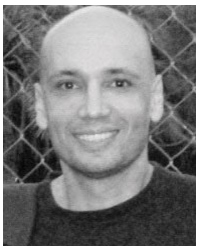

**ELI BARBIE** (Student Member, IEEE) received the B.S. degree *(summa cum laude)* in electrical and electronics engineering from the Shamoon College of Engineering, Beer-Sheva, Israel, in 2009, and the M.S. degree *(summa cum laude)* in electrical and computer engineering from Ben-Gurion University of the Negev, Beer-Sheva, in 2018, where he is currently pursuing the Ph.D. degree in electrical and computer engineering. Since 2015, he has been a Research Assistant with the Department of Electrical and Computer Engineering, Ben Gurion University of the Negev. His research interests include power electronics, multilevel converters, motion control, and harmonic mitigation in grid-fed converters.

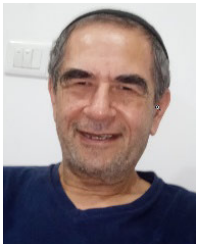

**RAUL RABINOVICI** was born in Iasi, Romania, in 1950. In 1979, he repatriated to Israel. In 2017, he retired as an Associate Professor with the Department of Electrical and Computer Engineering, Ben-Gurion university of the Negev, Beer-Sheva, Israel, while many years was responsible for the power systems specialization track. His research interests include low frequency magnetometry, simple magnetic field sensor for gamma-range fields, magnetometers, environmental 50 Hz magnetometry, nondestructive stress evaluation of ferromagnetic materials by magnetic methods, testing and evaluation of electro-magnetic devices, modern control of electric drives, and all aspects of energy conversion.

**ALON KUPERMAN** (Senior Member, IEEE) received the Ph.D. degree in electrical and computer engineering from Ben-Gurion University of the Negev, Israel, in 2006, while being with Imperial College London, as a Marie Curie Training Site Member. He was an Honorary Research Fellow with the University of Liverpool, from 2008 to 2009. He is currently with the School of Electrical and Computer Engineering, Ben-Gurion University of the Negev, where he is heading the Power and Energy Systems track and directing the Applied Energy Laboratory. His research interests include all aspects of energy conversion and applied control. He currently serves as an Associate Editor for *Energies*, IEEE ACCESS, and IEEE TRANSACTIONS ON INDUSTRIAL ELECTRONICS.